CAIT-UTC-017

Performance Determination of Precast Concrete Slabs Used for the Repair of Rigid Pavements

Final Report
October 2014

Reza S. Ashtiani, Ph.D.
Assistant Professor
University of Texas at El Paso
El Paso TX 79902

Gabriel de Haro
Graduate Research Assistant
University of Texas at El Paso
El Paso TX 79902

External Project Manager
Dr. German Claros
Texas Department of Transportation

In cooperation with
Rutgers, The State University of New Jersey
And
State of Texas
Department of Transportation
And
U.S. Department of Transportation
Federal Highway Administration

Disclaimer Statement

The contents of this report relfect the views of the authors, who are responsible for the facts and the accuracy of the information presented herein. This document is disseminated under the sponsorship of the Department of Transportation, University Transportation Centers Program, in the interest of information exchange. The U.S. Government assumes no liability for the contents or use thereof.

TECHNICAL REPORT STANDARD TITLE PAGE

1. Report No.	2. Government Accession No.	3. Recipient's Catalog No.
CAIT-UTC-017		

4. Title and Subtitle	5. Report Date
Performance Determination of Precast Concrete Slabs Used for the Repair of Rigid Pavements	October 2014
	6. Performing Organization Code CAIT/UTEP
7. Author(s) Reza S. Ashtiani, Gabriel de Haro	8. Performing Organization Report No. CAIT-UTC-017
9. Performing Organization, Name and Address University of Texas at El Paso 500 W University Ave El Paso, TX 79902	10. Work Unit No.
	11. Contract or Grant No. DTRT12-G-UTC16
12. Sponsoring Agency Name and Address Center for Advanced Infrastructure and Transportation Rutgers, The State University of New Jersey 100 Brett Road Piscataway, NJ 08854	13. Type of Report and Period Covered Final Report 1/01/13 - 10/1/2014
	14. Sponsoring Agency Code

15. Supplementary Notes
U.S Department of Transportation/Research and Innovative Technology Administration
1200 New Jersey Avenue, SE
Washington, DC 20590-0001

16. Abstract
The safety of civilians is of paramount importance during the construction and repair of concrete pavements. A complete understanding of the pavement distresses that compromise the structural stability and performance of rigid pavements are required for a proper selection of the repair method. Additionally, the time required to complete the repair process should be minimized to reduce the delay imposed on the users of the transportation facilities.
The US Air Force Research Laboratory (AFRL) in association with the Air Force Civil Engineering Support Agency (AFCESA) developed a state of practice protocol for the repair of damaged runways using precast concrete slabs. The current study tends to extrapolate the previous research on this topic to civilian highway pavements. In the AFRL study, three installation techniques, widely used by the transportation industry, were incorporated in the experiment design. The original study did not consider the influence of temperature fluctuations, humidity and the stresses induced by environmental conditions for the performance evaluation of the precast slabs. This study tends to capture the influence of the climatic conditions on the orthogonal llead bearing capacity of repaired sections.

17. Key Words	18 Distributional Statement
Precast slabs, Load transfer efficiency, Heavy weight deflectometer, Wrapping and curling stresses, Deformation energy	

19. Security Classification	20. Security Classification (of this page)	21. No. of Pages	22. Price
Unclassified	Unclassified	72	

Form DOT F 1700.7 (8-09)

Acknowledgments

Table of Content

List of Figures

List of Tables

1 Introduction

Rigid pavements are constructed to provide adequate support for loads exerted by transportation vehicles. Portland Cement Concrete (PCC) and adequate base and subgrade preparation is often implemented to reach a firm, stable, and smooth surface. After a determinate time of activity all rigid pavement require maintenance to ensure appropriate quality for their usage. It is imperative to restore traffic operations in the shortest possible time; therefore, the proper maintenance to utilize on damaged rigid pavements sections is controlled by the time specified for completing the task and the quality of repair required for each pavement structure.

Cast-in-place high-early-strength concrete and precast concrete panel installations are two methods to repair damaged rigid pavements. Both methods require completely removing the damaged portion of PCC airfield pavement and a replacement with an appropriate section. Cast-in-place entails placing fresh concrete into the resulting void after the extraction of the damaged portion. Traffic can be restarted in as little as 2 to 4 hours after installing. Cast-in-place method comes at the cost of intensive labor, skilled personnel is mandatory, the placement requires favorable weather condition, and high-early-strength rapid-setting concrete may not be as durable as traditional concrete [1].

Precast concrete panel methods offers advisable alternative to the cast-in-place method. The procedure requires the removal of the damaged section in a congruent dimension with a precast concrete panel already existing. Precast concrete repairs offer the possibility of completing the task in less than six hours if optimal climatic conditions are present allowing the traffic to be reopen in a short period of time [2]. Quality control is higher on precast panels since they are manufactured in a controlled environment. The exposed surface can be texturized in a clinical environment. The curing is done in an environmentally control area and the panel can be stored on site until needed. In addition, the weather window required for installation of precast panels is larger than the one for cast-in-place repairs [2].

Nevertheless the cost is usually high, transportation agencies have estimated the cost of precast concrete panels repair to be 1.6 to 4 times higher than the cast-in-place repair method [2]. The life expectancy and performance of precast panels has not been fully understood being that precast repair methods are a relatively recent technology and there is not enough research.

Factors determining the service life of a rigid pavement are frequency and the type of transportation vehicles, base-course, sub-grade, environmental, and temperature conditions. Maintenance on the damaged sections is required once the deteriorating effects begin to emerge in a pavement structure. Appropriate maintenance can be perform in minor damaged areas avoiding traffic interruption. However, repairs in pavement areas containing single or multiple slabs require special techniques and organization to minimize the impact on the traffic operation.

Fast-tracks techniques are high-quality and long-lasting repairs intended to restore severely damaged rigid pavements reducing traffic operational delays. These techniques involve the entire removal of a damaged portion of pavement structures and replacing it with a new section.

1.1 Objective

Rigid pavement conditions deteriorate as their usage and time of life increases. When restoring rigid pavements an efficient and feasible technique should be carry out to ensure the least possible time delays and high quality performance; therefore, this study focus on precast repair panels rather than cast-in-place. Recently, a practice protocol for the repair of damaged runways using precast concrete slab was develop by the United States Air Research Laboratory (AFRL) in collaboration with the United States Air Force Civil Engineering Support Agency (AFCESA) [3]. The study evaluated the effects of construction techniques and the material performance of the repair section. Environmental factors such as temperature and humidity were neglected on the evaluation of the repaired section.

The Outcomes of this research will support the United State Department of Transportation (USDOT) goals and priorities. Better understanding in the repair of concrete field will be accessible to the transportation consortium and the safety and economic competiveness will be improved. The research will provide a mechanistic approach using computational mechanics and non-destructive field-testing to evaluate the impact of curling and wrapping stresses on the performance of precast concrete panels. Transportation community will understand better the behavior of precast concrete panels in different environmental conditions. Climatic data will be considered in a comparative analysis of technologies for the repair of rigid pavements. Greater understanding of the behavior of concrete repair panels will result in alternative techniques for construction and proper material usage to minimize the delays for the user of the transportation facilities, improving safety, and economically ways of repairing damaged concrete slabs.

1.2 Approach

Tests on Precast Portland concrete cement (PCC) repair panels were executed and the decay of the performance was monitored at certain load intervals to evaluate the effects of temperature variation on the mechanical performance of severely damage rigid pavements. The synergic impact of loads induced and temperature stresses on the mechanical performance of the repaired section were monitored. The precast panels were subjected to accelerate field loadings to simulate the synergic impacts induced by the movement of transportation vehicles. Performance plots were prepared for field practitioners to efficiently and economically select the best available combination of repair techniques and leveling with respect to climatic data.

A Heavy Weight Deflectometer (HWD) was used to back-calculate the layer modulus in the approaching and departing slab. The non-destructive test data at the two sides of the joints was used to characterize the deflection-based load transfer efficiency of precast slabs for each variation of the experimental design. The factors influencing the performance of the experiment design were taken from a robust statistical analysis on field measurements. Performance degradation plots for each permutation of the experiment design were done. Comparative performance analyses of precast slabs were used as a

performance measure using the gradient of the performance curves. Performance criteria such as joint stiffness and dissipated deformation energy in the subgrade were considered to deliver a comprehensive analysis of the performance of repaired section using precast concrete panel.

Collected data for different leveling bonding material agents was used to study the impact of material properties on the temperature dependency of the precast slabs. Air Force Civil Engineering Support Agency (AFSEASA) selected and tested the bonding agents to meet with the Unified Facilities Criteria (UFC) requirements. Polymer-based agent and a cementitious fill were considered for the analysis. Fort Miller Super-Slab, URETEK and Michigan methods of construction were considered for the data since they are traditionally used by the transportation industry. Direct injection of high density polymer (HDP) foam underneath the slabs, deep injection of HDP foam 3 feet deep into the subgrade, and conventional flowable fill installations were the techniques used for comparison. HWD data was collected once the repair concrete was installed and after certain loading intervals. HWD data collected in the field were used to determine the material properties and joint stiffness of the PCC slabs. Finite element analysis was then used to calculate the pavement responses in a more detail approach.

HWD data and temperature profiles for a span of 8 hours of a hot summer day were used for back-calculation of the material properties in the pavement layers. A quadratic equation was used to simulate the nonlinear dissipation of temperature through the pavement structure. Stress-based load transfer efficiency plots were generated for comparison of each section. An HWD test at two sides of the joints was performed to calculate the deflection-based load transfer efficiency of the concrete slabs.

The deformation energy dissipated to the subgrade caused by accelerated loading conditions was determined. Using the deformation energy data, plots of the decay of subgrade stiffness were plotted with the number of load applications increasing. With these data conclusions for better-quality construction technique and bonding agents for a specific environment can be identify.

2 Background

2.1 Installation Methods

Several methods exist to repair rigid pavements using precast concrete panels. The most common practice methods in the transportation industry are the Fort Miller Super-Slab Method, the Michigan Method, and the URETEK Method [2]. The difference between the three methods is the variation in the installation techniques. It is imperative to state that the usage of precast concrete panels with equivalent dimensions as the removal portion of the damaged slab is a similarity share among the three methods.

2.1.1 Fort Miller Super-Slab Method

Fort Miller Super-Slab method consists of installing precast concrete panels that have the exact dimensions as the damaged section previously removed from the existing slab. The mechanical properties on the layer underneath both sections must match. In addition, dowels are used as load transfer mechanisms to connect the precast concrete repair panel to the original slab. Figure 1 display the single or multiple installations of slabs.

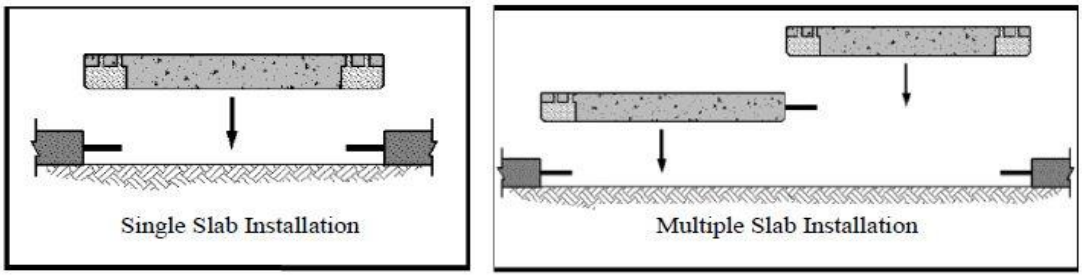

Figure – 1 Fort Miller Precast Concrete Repair Panels [3]

2.1.1.1 Load Transfer

Fort Miller Super-Slab load transfer mechanism consist in connecting the existing concrete slab with steel dowels to the precast repair panel. The precast concrete repair panel has to be fabricated with dowel sleeves on bottom of the panel. Accurate configuration for the sleeves and the load transfer dowels has to be arranged in order for correct installation. Grout ports are provided as well to grout the dowels after placing the precast concrete panel. The process is shown in Figure 2 and Figure 3 [4].

Figure – 2 Preparation of Existing Slab and Installation of Precast Repair Panel [4]

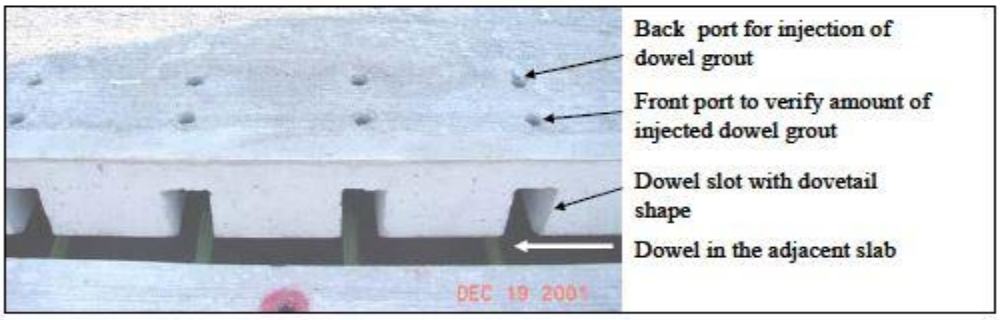

Figure – 3 Adjustments in Slabs for Proper Installation [4]

2.1.1.2 Preparation of Base

Base course material has to be compacted and a 3/4-inch-thick-layer of fine mineral material aggregate needs to be spread over the base. Specialized grading equipment to screeds the base surface needs to be used for accuracy. The bedding is injected under the panel once the base is prepared, and once dowels are placed in the correct position. Channels under the precast panel are provided for proper distribution of the bedding grout. Figure 4 illustrates the procedure of installing a precast concrete panel.

Figure – 4 Installation of Precast Concrete Panel [4]

2.1.2 Michigan Method

The Michigan Department of Transportation developed a method called the Michigan Method. It was mainly designed for full-depth highways pavements repairs; however, the Michigan Method can be implemented in other transportation infrastructures [5].

2.1.2.1 Load Transfer

The technique of dowels casted into the precast concrete panel and dowel slots cut into the existing concrete slab is used to accomplish a satisfactory load transfer. Three dowels in each wheel path are placed, each one spaced 1-foot apart. Adequate dimensioning between the dowels slots and the dowel bars are required for proper fitting. Figure 5 illustrates the installation technique as well as the transfer mechanism.

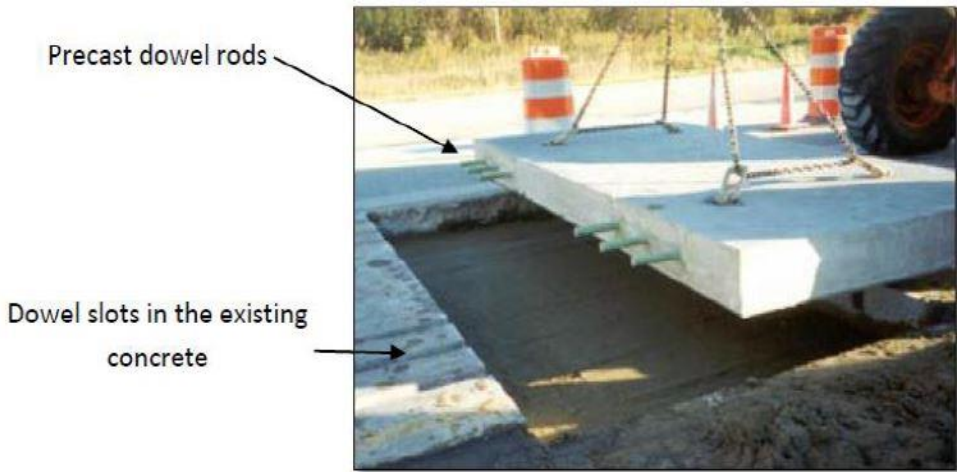

Figure – 5 Load Transfer Dowels and Dowel Slots [5]

2.1.2.2 Preparation of Base

Flowable fill is employed for the base preparation. Flowable fill is a mixture containing Portland cement, water, fly ash, fine mineral aggregate and ½-inch or smaller coarse mineral aggregate. The flowable fill is mixed and delivered to the job site in ready mix truck. Subsequently, after a well compaction is performed in the base layer, the flowable fill is placed above to guarantee complete panel seating and leveling.

Figure – 6 Flowable Fill Being Place [5]

2.1.3 URETEK Slab Method

URETEK slab method is a patented method involving the controlled injection of high-density polyurethane (HDP) foam under the concrete slab for lifting and leveling purposes. Fiberglass ties are implemented as load transfer mechanisms.

2.1.3.1 Load Transfer

The load Transfer is handle by utilizing specially manufactured fiberglass ties as load transfer mechanisms (Figure 7) [6]. Once the precast panel is placed the fiberglass ties are installed. The ties are inserted and grouted to connect the existing and the repair concrete slab. In Figure 8 the installation

process for the fiberglass ties is illustrated.

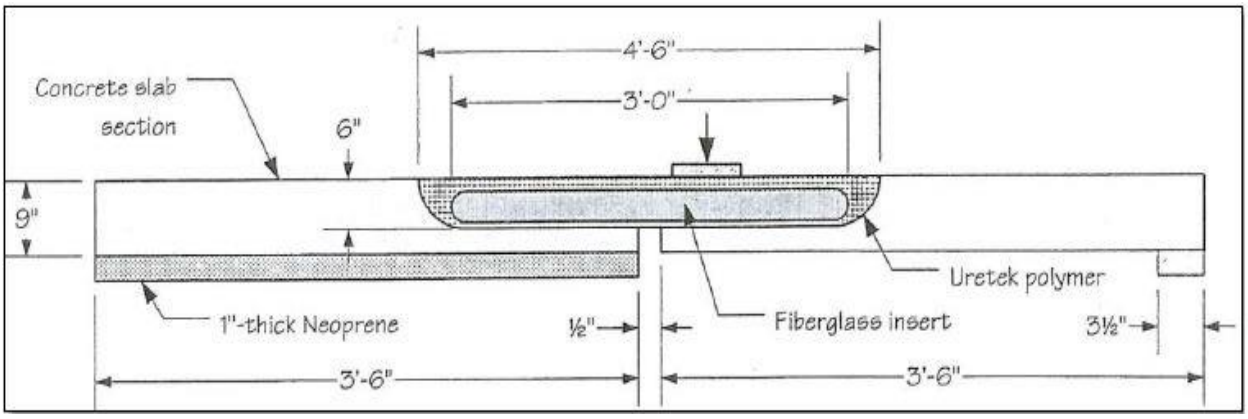

Figure – 7 Illustration of Fiberglass Ties [6]

Figure – 8 Fiberglass Tie Installation [6]

2.1.3.2 Preparation of Base

The base preparation technique for the URETEK Method is a process where HDP foam is injected through the precast concrete panel using 5/8-inch diameter drill holes. Generally the holes are spaced uniformly trough the repaired section. Several full-depth portholes are made to facilitate the foam distribution. The URETEK base preparation relies on control chemical expansion. Once HDP foam is injected through the drill holes, precise leveling equipment is used to ensure the material does not spread beyond the desired area. Upon injection, the HDP immediately expands to lift, re-support and accurately realign concrete repair slabs. Voids underneath the repair concrete slab are quickly filled and the expansion of the HDP gently raises the slab as desired. The HDP quickly cures into a strong and stable base material.

Deep injection of HDP foam is an alternative technique to use the URETEK method. This alternative technique requires drilling portholes several feet into the sub-grade. HDP foam is then injected into the sub-grade filling all voids or fissures while compressing and densifying the soil. The Injection of the HDP foam forces the precast concrete repair panel to raise upward as it is injected. In order to achieve an accurate leveling, precise leveling equipment is used to align the slabs. Figure 9 show from left to right the portholes drilling, injection of HDP foam and leveling equipment.

Figure – 9 URETEK Method Installation Technique [3]

2.2 Fabrication of Precast Concrete Repair Panels

The fabrication technique and the dimensions for the precast concrete repair panels are describe in this section. In addition, this section describes the load transfer mechanisms that were installed during the fabrication of the precast concrete repair panels.

2.2.1 Mold and Dimensions for Precast Concrete Repair Panels

Although three repair concrete panels were installed using different techniques, the manufacture for all three were identical. A 9-feet 10 ½-inches square steel form was designed and constructed for the fabrication of the precast concrete repair slabs. The dimension of the precast concrete repair slabs guaranteed a ¾-inch construction joint between each edge of the precast concrete panel and the existing slab. The frame included longitudinal dowels slots at both ends for pre-installation of dowels prior to fresh concrete placement. Exteriors dowel were placed as well in the steel frame to ensure alignment during concrete placement.

The test pad (existing slab) consisted of 12-inches thick PCC. The precast concrete repair panels were fabricated with a thickness of 9-inches. The length and wide of the repair panels consisted of 9-feet-10 ½ inches with reinforcement dowels at east and west bounds as load transfer mechanisms. A space of ¾-inch was left for accommodation of joints between each edge of the precast concrete panel and the existing slab.

2.2.2 Load Transfer Mechanisms

Dowels bars installed in the repair panel prior to concrete placement were placed to server as load transfer mechanisms. Additionally, dowels slots were cut in the existing concrete slab with similar dimensions for assembly. Dowels with 1-inch in diameter and 22-inches long were installed in the precast repair concrete panel as load transfer mechanisms. The longitudinal dimension of the dowels were place such that 11-inches were inside the precast panel and 11-inches left to connect to existing concrete slab. The dowels were centered 4 ½-inches from the top surface. Each dowel rod was space 1-foot apart of each other with the first dowel located-6 inches from the edge of the precast panel.

The repair concrete panels were fabricated with a 3/8-inch diameter rebar (#3) reinforcement grid arranged in a 1-foot by 1-foot square pattern. The reinforcement gird purpose was to mitigate concrete cracking attribute to transportation. A 3/8-inch concrete cover was placed between the ends of the

reinforcement bar and the side of the frame. The gird was placed 1 ¼-inch rebar from the bottom of the precast panel, leaving a rebar depth of 7 ¾-inches from top surface of the precast panel. Figure 10 shows the rebar grid installation, the load transfer dowels, and the dowels placed to align firmly the steel frame.

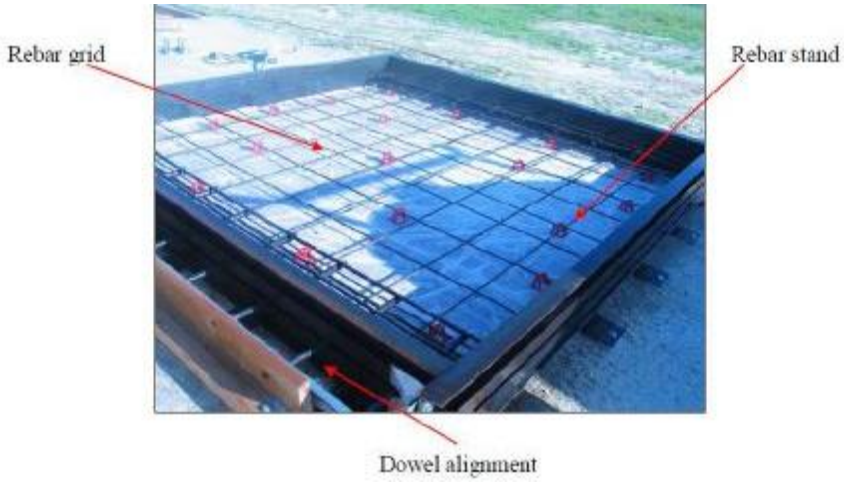

Figure – 10 Precast Concrete Panel Fabrication [3]

3. Methodology of the Experiment

Three pre-cast concrete panels were installed using different techniques for comparison purposes in the analysis. Conventional HDP foam, HDP foam deep injection and flowable fill were the pre-cast installation techniques used for slab #1, Slab #2, and Slab #3, respectively. The base preparation and concrete mix design were also different for each panel. Figure 11 shows a top view of the existing concrete slab and location of the repair sections for each precast concrete slab.

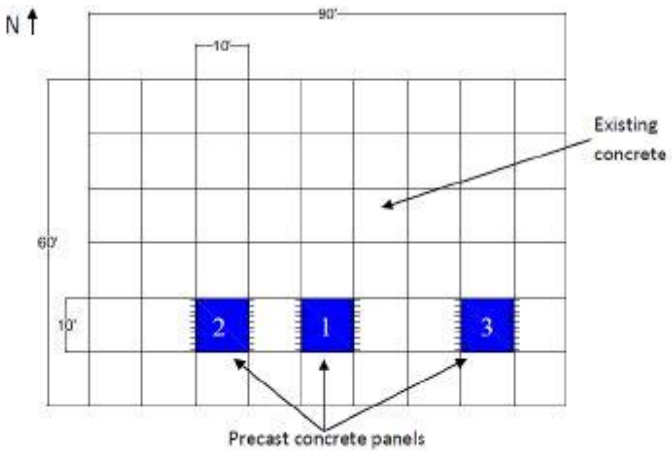

Figure – 11 Precast Concrete Panels Locations [3]

3.1 Slab Removal and Dowel Slots Sawing Process

Two different equipment were used to saw the distress portion of the existing concrete slab. A wall saw which operates on a rail system and a walk behind concrete saw. Nowadays, most of the companies only have one type of equipment to saw concrete slabs; therefore, this report will not emphasis in any specific equipment for the sawing process.

Once the distressed portion of concrete slab was trim, swift-lift attachments were installed. The swift-lift attachments were installed by removing four 6-inches in diameter full depth cores from the sawed section. Pavemend 15.0 rapid-setting cementitious grout was placed in the removed area and the lifting attachments were inserted in the freshly placed grout. The stress slab portion was removed 2 hour after installation of attachments since the required PCC compressive strength for lifting the attachments was 1,600 for each point and the specification stated that the grout could reach compressive strength of 2,500 after 2 hours [7]. The Distress portion removal was completed once the lifting attachments were connected and secured into a mobile crane. Figure 12 illustrates lifting attachments already installed and the mobile crane removing the distress slab portion.

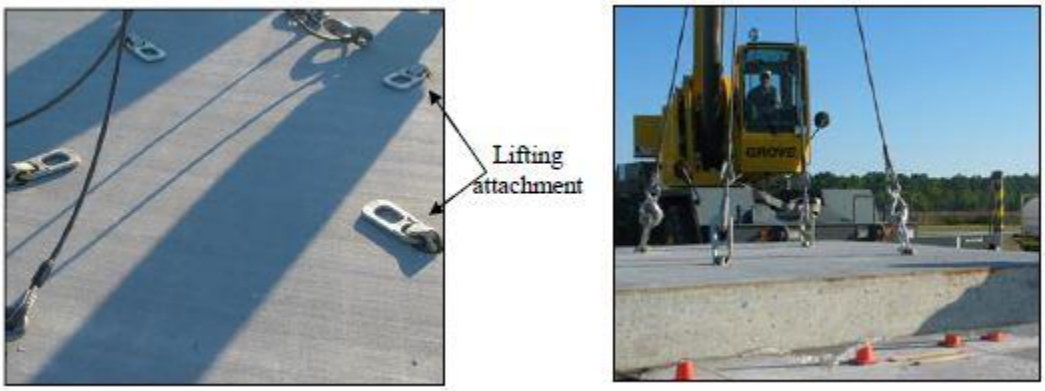

Figure – 12 Distress Portion of Slab Removal [3]

Slots were sawed in the existing concrete slab for a correct assembling of the load transfer mechanisms. The existing slab modifications were done using a walk-behind concrete saw for the cutting of the perimeter portion of the dowel sleeves. A jackhammer was used to chisel and to remove the inner portion of the cutout sleeves. The slab removal procedure described was implemented for the three precast slab installations. The figure 13 displays the procedure.

Figure – 13 Dowel Slots Sawing Process [3]

3.2 Concrete Mix for Repair Slabs

Although the fabrication of the three concrete repair slabs was done with the same dimensions and load transfer devices, only slabs #1 and #2 shared the same concrete mix. Slab #3 was fabricated with concrete mix carrying different property materials. Slabs #1 and #2 was constructed with a specified 28-day compressive strength of 5,000 psi, while slab #3 was constructed with Albright heat resistance concrete. Albright heat resistance concrete can achieve a 28-day compressive strength of up to 6,000 psi in accordance with ASTM C 39 (Standard Test Method for Compressive Strength of Cylindrical Concrete Specimens). Albright concrete design mixture was originally designed to resist concrete degradation caused by extreme temperatures emitted by the thrust of military aircraft.

3.3 Base Preparation

Two different base preparations had to be done. The base preparations required before installing panel #1 and #2 were similar; however, base preparation for precast repair panel #3 had to be done differently since there were problems once installing the repair panel. The original concrete slab consisted of 12-inches in thickness and the precast concrete repair slab was 9-inches.

3.3.1 Base Preparation for Panels #1 and #2

Once the original PCC slab was removed a void with 12-inches in depth was created. Additionally 4 extra inches of existing base-course material was excavated leaving a void with 16-inches in total depth. The 16-inches thick void was partially filled with a new 6-inches-thick well-compacted crushed-aggregate base course layer. The main purpose for removing base and then replacing it with a well-compacted new material was to mitigate the settling beneath the precast panel when installing the precast repair panels. After the new base course layer was constructed a void with a 10-inches depth was still remaining. 9-inches of the void was occupied by the precast concrete repair panel leaving 1-inches for leveling purposes. The leveling technique used for the installation of slab #1 and #2 was done using URETEK HDP foam. The process for installation of slab #1 and #2 is describe later in Section 3.4.

3.3.2 Base Preparation for Panel #3

The base preparation was done twice for panel #3 since in the first attempt the existing and the repair concrete panel did not end up level. The first attempt was done similarly to the one for slab #1 and #2. New base was constructed after removing 12-inches in thickness of the damaged portion of concrete slab with an extra 4-inches of existing base-course material. The resulting void was then filled and compacted with the 6-inches of new base material, leaving a void of 9-inches in thickness. The remaining void was filled with 1 ½-inches of flowable fill leaving 8 ½-inches as the remaining void. The precast concrete repair slab thicknesses were of 9-inches; however, only spaces 8 ½-inches were left for their installation. This was done since an assumption was made that the layer of flowable fill place was going to compact. Figure 14 displays a side view of the set up for the unsuccessful attempt of installation of the precast concrete panel.

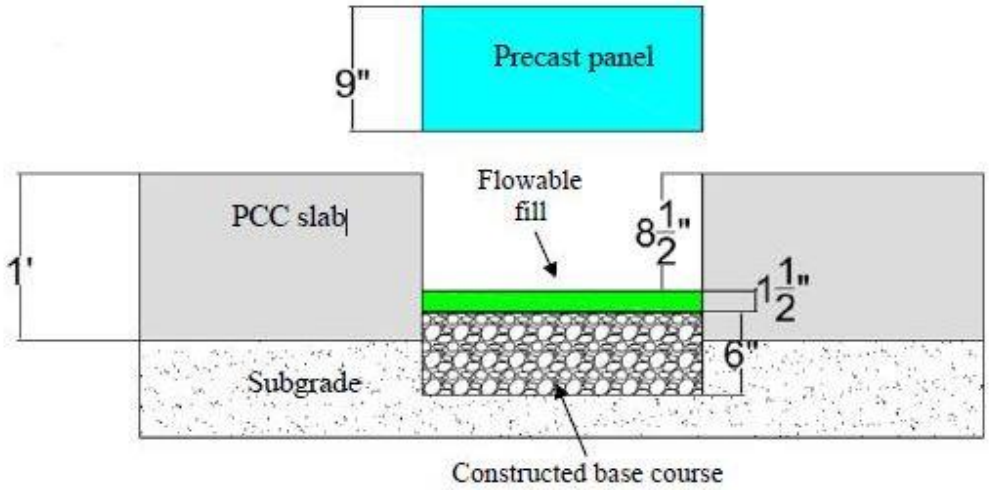

Figure – 14 Unsuccessful First Attempt for Base-Course Preparation Configuration [3]

The precast concrete repair slab was installed immediately after the pouring of the flowable fill but the flowable fill compression was not enough. The precast repair panel came to rest approximately ¼-higher than the existing PCC concrete slab. The unsafe scenario created by the not level portion in the slab results in a relatively impermeable environment and in a bump in the concrete road which was a potential source for sliding of tires or a moment creator in transportation vehicles. The precast concrete panel installation was not acceptable and was removed with the help of a crane. The freshly place flowable fill and the 6-inches in thickness layer of new constructed base course were removed as well.

After removing the previous base preparation and the precast repair concrete slab, a new base course layer was constructed for the second attempt. In this case the 16-inches in thickness void was fill with a 3-inches-thick well-compacted crushed-aggregate base layer. The remaining 13-inches of void were fill with the 9-inches from the precast concrete repair panel and with 4 ½-inches of flowable fill material. Although, after placing the 4 ½-inches thick of flowable fill there was only a remaining of 8 ½-inches for the precast repair panel, by only placing 3-inches of new base course material it ensure 1-inch of flowable fill layer to be surrounded by soil. The soil surrounding allowed the flowable fill to have a large compression capability.

The second attempt for installing precast panel 3 was successful. The flowable fill compressed a satisfactory quantity to level with the existing concrete slab. The Flowable fill properties are described later in this report in the installation of the panels section (Section 3.4.3). Figure 15 illustrates the successful attempt for base-course preparation**.**

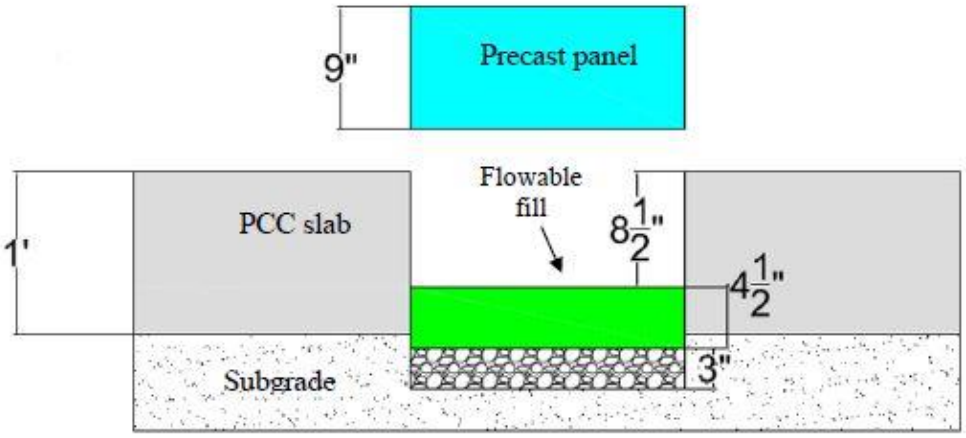

Figure – 15 Successful Second Attempt for Base-Course Preparation Configuration [3]

3.4 Installation of Panels

The three methods of installation evaluated in this report are described in detail in this section. Concrete repair panel #1 was installed with conventional injection of HDP foam, concrete repair panel #2 with deep injection of HDP foam into the subgrade and concrete repair panel #3 with flowable fill. The installation of each panel was done after the base preparation required for each slab.

Once the base preparation and the installation of the panel were done the ¾-inch joints were sealed with Pavemend 15.0. Pavemend was placed along each edge of the panel until the joints and dowel sleeves were completely filled. The freshly placed grout was brushed and finished using hand tools. The lifting points and injection portholes were left un-grouted. The joint sealing procedure was performed for the three repair panel installation. The joint sealant procedure finalized the installation procedure of the repair concrete slabs.

3.4.1 Precast Repair Panel #1 (Conventional URETEK HDP foam Installation)

The installation of the precast concrete slab #1 was performed using URETEK high density polyurethane expanding foam to level and support the precast panel. URETEK HDP foam was injected directly underneath the repair concrete panel through portholes drilled after the panel placement. Survey measurements were required at each corner of the precast concrete panel to determine the differential heights between the existing PCC concrete slab surface and the precast concrete repair surface. The survey measurements obtained were the following:

a) NW corner – 5/8 inch below the PCC surface
b) NE corner – 1 inch below the PCC surface
c) SW corner – 1 inch below the PCC surface
d) SE corner – 1 ¼ inch below the PCC surface

Prior the leveling process between the two slabs URETEK HDP foam was injected along the bottom perimeter of the precast concrete repair slab to create a seal. The purpose of sealing the edges of the

precast concrete panel was to prevent the foam from blowing out to the sides during the injection operation. Subsequently, the URETEK HDP foam was injected into the precast concrete slab while measurements were taken at each corner of the precast concrete until the existing and precast panels were level properly. The URETEK HDP foam was injected through nine 3/4-inch diameter injection ports drilled through the precast concrete repair panel.

The precast repair panel uprising was monitored with precision laser-leveling equipment placed near each corner of the precast concrete panel. The monitoring was performed to accurately terminate the injection of HDP foam when the precast panel was precisely level with the existing slab. The layout of the injection ports in the precast panel is display in Figure 16.

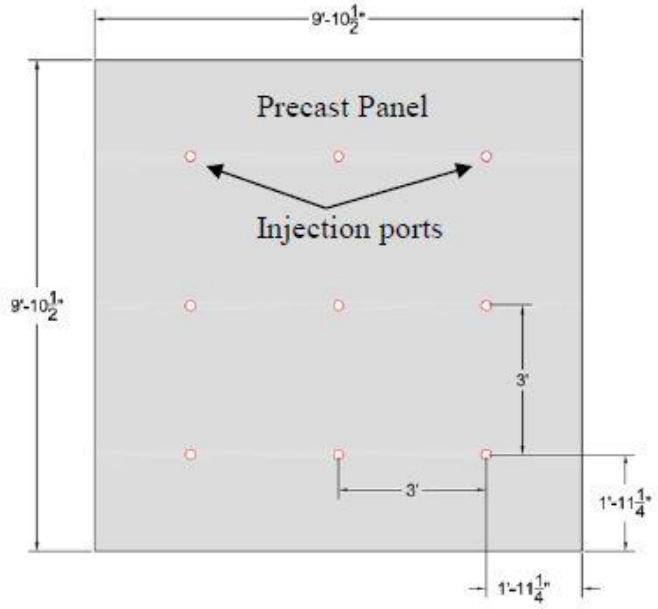

Figure – 16 Precast Panel Injection Ports Layout [3]

3.4.2 Precast Repair Panel #2 (URETEK HDP foam Deep Injection)

The installation of the precast concrete slab #2 was similar to precast concrete #1 using URETEK high density polyurethane expanding foam; however, the jacking/leveling for panel #2 was done by injecting the URETEK HDP foam 3-feet into the sub-grade. Surveying measurements to determine the height differential between the existing concrete slab and the concrete repair panel were taken to determine the amount of HDP foam required. The results were the following:

a) NW corner – 1 3/8 inch below the PCC surface
b) NE corner – ½ inch below the PCC surface
c) SW corner – 1 inch below the PCC surface
d) SE corner – level with the PCC surface

Panel #2 had the same layout configuration of portholes as panel #1 (Figure 16) with only an addition of an extra injection porthole place 2-inches apart from every porthole used for slab #1. The purpose of

adding an extra porthole was to use one for deep injection of the foam and the extra porthole to use it as a shallow injection point. The deep injection portholes purpose performed most of the leveling work and the shallow injection portholes was mainly for precision leveling. The drilling of the deep portholes was performed using ¾-inch diameter shaft. The deep portholes were drilled through the precast panel plus 3-feet into the sub-grade material. A ¾-inch diameter hollow metal rod was inserted into the drilled cavity for collapse prevention. The joints and dowels sleeves were grouted for the final installation of the precast concrete repair panel.

3.4.3 Precast Repair Panel #3 (Flowable Fill)

The precast repair panel #3 was not installed with URETEK HDP foam, instead the panel was installed using flowable fill placed below the precast concrete repair slab. Flowable fill is a concrete mix composed of Portland cement, fly ash, fine mineral aggregate and water. The flowable fill mixture was designed by a local ready-mix plant and was transported and placed with the help of a ready mix concrete truck.

The precast concrete panel was installed immediately after the flowable fill placement to avoid any possible curing of flowable fill. Each panel corner was equipped with a steel plate to prevent the risk of panel sinking into the flowable fill. The plates were mechanically connected to the top of the surface of the precast panel. They were oriented to overhang a portion on each side of the panel corner to connect the surfaces of the precast panel and the adjacent PCC. Rapid-setting grout was used to seal the joints and the dowels sleeves as the final procedure in the installation of the precast repair panel #3.

3.5 Timelines for Installation of Each Concrete Slab

The timelines for removal of existing damage portion, fabrication of precast concrete, and installation of the repair precast slabs were recorded and compared. This since the rapid restoring of the transportation flow is crucial when constructing or repairing an area. The times required for a fully installation were recorded and measured for each concrete repair slab separately. Subsequently, the times measured for every task were added and compared to choose the most feasible. The results are based in the time required to complete each task and they reflect the feasibility and efficiency of each method.

Tables were created for every precast concrete repair installation technique. Tables 1, 2 and 3 display the timelines for installing precast concrete repair panels #1, #2, and #3, respectively. Table 4 shows the time required to perform the distressed slab removal when a wall-saw is employ, and table 5 the time required when a walk-behind concrete saw is employ. Furthermore, table 6 shows the panel fabrication timeline, and table 7 the precast concrete panel transportation timeline.

Table 1. Timeline for Precast Concrete Panel 1 Installation, URETEK Direct Injection

Task	Time (minutes)
Dowel slot cutting/removal (existing PCC slab)	60
Base course excavation	60
Base course construction	60
Precast panel placement	15
Porthole drilling operations	45
URETEK injection and leveling operations	60
Placement of joint and dowel fill material	30
Rapid-set finishing	5
Total	335

Table 2. Timeline for Precast Concrete Panel 2 Installation, URETEK Deep Injection

Task	Time (minutes)
Dowel sleeve excavation (existing PCC slab)	60
Base course excavation	60
Base course construction	60
Precast panel placement	15
Porthole drilling operations	90
URETEK injection and leveling operations	60
Placement of joint and dowel sealant	30
Rapid-set finishing	5
Total	380

Table 3. Timeline for Precast Concrete Panel 3 Installation, Flowable Fill

Task	Time (minutes)
Dowel sleeve excavation (existing PCC slab)	60
Base course excavation	60
Base course construction	60
Flowable fill placement (simultaneous with slab install)	20
Precast panel placement	15
Placement of joint and dowel sealant	30
Rapid-set finishing	5
Total	250

Table 4. Timeline for Wall-Saw Distressed Slab Removal

Task	Time (minutes)
Mark perimeter of distressed slab	20
Saw-cutting operations	240 (four sides @ 60 minutes each)
6-inch-diameter coring operations	20 (four cores @ 5 minutes each)
Rapid-set mix and placement	10 (four cores @ 2.5 minutes each)
Swift lift installation	5 (four anchors)
Rapid-set cure time	15 (Temp/weather variant)
Attach crane rigging hardware	5
Extract distressed slab	10
Total	325

Table 5. Timeline for Walk-Behind Concrete Saw Distressed Slab Removal

Task	Time (minutes)
Mark perimeter of distressed slab	20
Saw-cutting operations	80 (four sides @ 20 minutes each)
6-inch-diameter coring operations	20 (four cores @ 5 minutes each)
Rapid-set mix and placement	10 (four cores @ 2.5 minutes each)
Swift lift installation	5 (four anchors)
Rapid-set cure time	15 (Temp/weather variant)
Attach crane rigging hardware	5
Extract distressed slab	10
Total	165

Table 6. Timeline for Precast Concrete Panel Fabrication

Task	Time (minutes)
Form set-up	240
Rebar cutting operation	20
Rebar mat fabrication	60
Dowel placement and alignment	60
Concrete placement	10
Concrete finishing	45
Swift-lift insertion	5 (four anchors)
Total	440

Table 7. Timeline for Transporting the Precast Panel

Task	Time (minutes)
Attach rigging hardware	5
Lifting operation (from constructed site to truck)	15
Lifting operation (from truck to repair area)	15
Total	35

According to the times previously presented in Tables 1, 2, and 3, the flowable fill resulted in the smallest among the three installation methods. Although the installation time was the smallest, the comparison among the three did not took into account the difficulty when installing flowable fill. As discussed in Section 3.3.2, the difficulty to pre-determine the requisite volume of flowable fill necessary could affect negatively the installation procedure by increasing the installation timeline.

The distressed slab removal was faster when the walk-behind concrete was employed. The walk-behind saw operation required 165 minutes to complete the task, while the wall-saw operation took 325 minutes. The times were reduced almost by half; however, the necessity of experienced operator is required for the walk-behind operation. The panel fabrication and transportation of precast panel timelines were also displayed in tables 6 and 7, respectably.

4 Concept and Assumptions

4.1 Warping and Curling Stresses

Warping and Curling stresses are cause by temperature changes on the concrete slab. During the day, when temperature at the top of the slab is greater than at the bottom, top part expands while the bottom tends to contract. The weight of the concrete slab restricts it from expansion or contraction; therefore, compressive stress and tensile stress are induced at top and bottom of the slab respectively. During night, when temperature on the top part of the slab is lower than at the bottom, the expansion, contraction and stress are the opposite than during the day. Tensile and compressive stresses are induced at the top and bottom part of concrete slab respectively.

Figure 17 Illustrates a typical curling and warping stresses distributions due to temperature gradient in daytime and nighttime. The Figure (a) shows the typical nighttime curling of the PCC layer as the top fiber of the concrete pavement is cooler than the bottom fiber; therefore it has a bowl shape. Figure (b) shows a typical day time curling were it is the other way around, top layer of PCC is warmer than the bottom layer, therefore the concrete slab deformation resembles a dome.

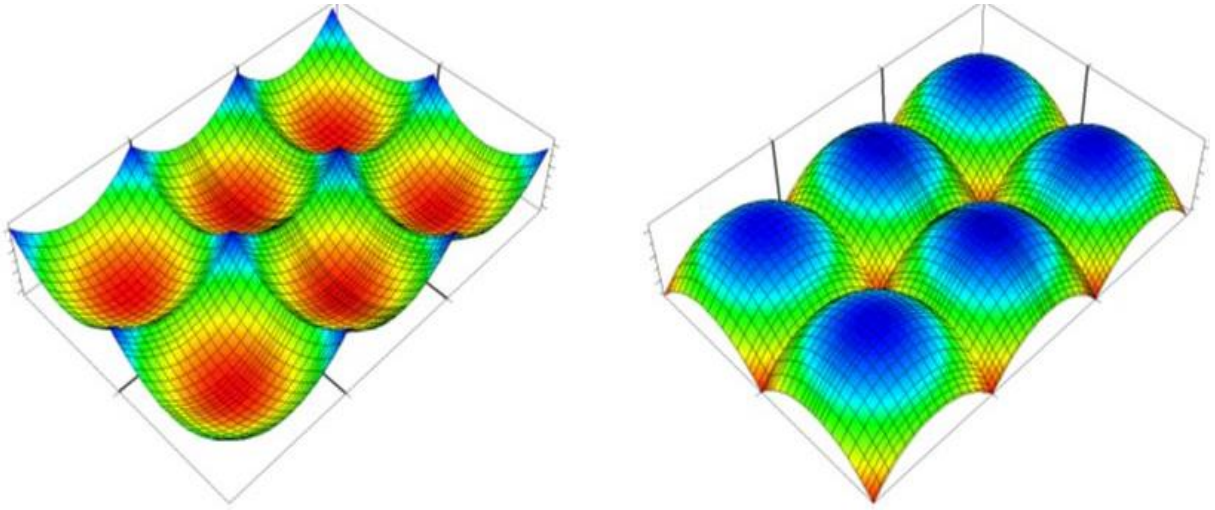

(a) Night Time Curling **(b) Day Time Curling**

Figure – 17 Difference between Night Time and Day Time Curling [3]

4.2 Design Factor (Stress/Strength)

Vertical Stress (σ_v) and Strength of concrete are frequently used to evaluate the performance of highways and airport pavements. The vertical strain is caused mainly by the vertical stress, the horizontal stress is relatively small; therefore, the vertical stress is used for the design factor calculations. The concrete modulus of rupture (S_c) is the other parameter for calculating the design factor since it characterizes the bending strength or the fracture strength of the concrete slab.
The ratio between maximum vertical stress and the modulus of rupture is defined as the design factor. Design factor can be seen as the factor of safety; however, the design factor is a parameter a pavement structure required to satisfy for proper functionality of the pavement structure. The factor of safety parameter can be higher than the design factor as much as desired. The calculation of the vertical stress is done with the help of a Heavy Weight Deflectometer (HWD) equipment. The application of an HWD device is describe in Sections 4.7 and 5.1.The concrete strength is calculated using the compressive strength of concrete (f'_c). The concrete strength can be calculated using Equation 1 [10].

$$S_c = 6.5\sqrt{f'_c} \quad (1)$$

The calculation of the compressive strength (f'_c) is first required to use Equation 1. The compressive strength is calculated using Equation 2. The modulus of elasticity of the concrete selected for the test is required to calculate the compressive strength parameter (f'_c).

$$E_c = 57000\sqrt{f'_c} \quad (2)$$

The ratio stress/strength has to be performed for all the concrete panels being evaluated. A lower ratio means a more effective pavement structure since the stress/strength ratio required for a satisfactory performance is small. On the other hand the higher values of strength ratio corresponds to pavement

systems that are more prone to develop distresses during the service life.

4.3 Load Transfer

According to AASHTO the term “Load transfer” refers to the distribution of load across discontinuities such as joints or cracks. In the mechanistic analysis and design of precast panels load transfer is a crucial parameter since the purpose of the repair panel is to keep the slab performance as if it was still one structure without any discontinuities for optimal performance.

Load transfer is influenced by factors such as loading conditions, foundation support, load transfer mechanism (aggregates and dowel bars), temperature, joint spacing, and stiffness and thickness of the concrete slab [8]. Loading condition refers to the type and loading duration, bigger and larger duration results in greater load to be transfer. Foundation support is referred to the base and subgrade layers supporting the concrete slab. Poor quality material or bad compaction of foundation will result in loss of foundation support leaving the load transfer devices with more loads to handle. Joint opening caused by temperature gradient refers to the shrinkage characteristics of the concrete when subjected to different temperatures. Joint spacing depends on the type of aggregate and climate of the zone. As joint spacing increases, the aggregate interlock decreases, and there is also an increased risk of cracking. In addition, the stiffness properties and thickness of the concrete slab will also affect the load transfer performance of the concrete sections. The function of a load transfer mechanism is to reduce as much as possible the plastic deformation of the loading slab $(\varepsilon_p)_l$ and unloading slab $(\varepsilon_p)_{ul}$. Figure 18 illustrates the function of load transfer mechanisms for two concrete slabs when a moving load is applied to the rigid pavement structures. Additionally, vertical stresses at the loaded slab $(\sigma_v)_l$ and unloaded slab $(\sigma_v)_{ul}$ is shown in Figure 18. The responses at the joints are usually used to characterize the efficiency of load transfer devices and installation methods for rigid pavements structures.

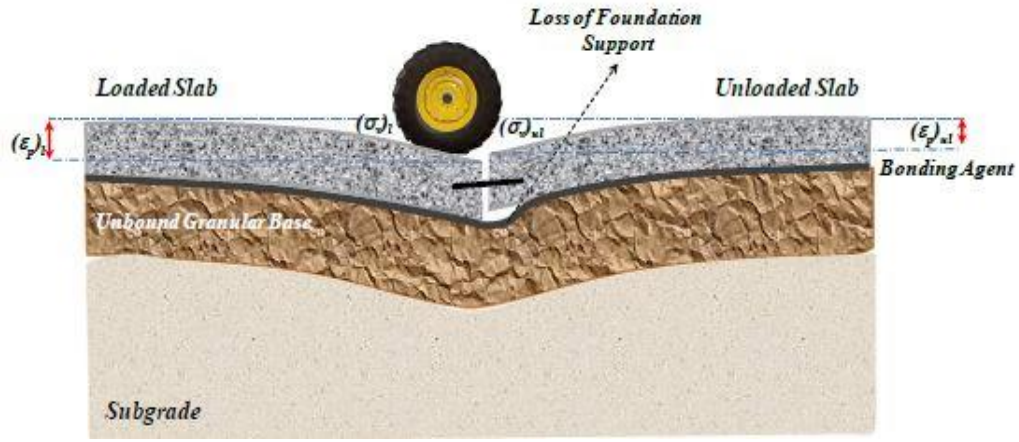

Figure – 18 Load Transfer Mechanism in Rigid Pavement [3]

4.4 Load Transfer Efficiency (LTE)

When a moving heavy load passes over a connecting joint of a concrete pavement, the departure and approaching slabs deforms due to load transfer between the slabs. The implementation of dowels and tie bars maximize the load transfer efficiency when connecting two concrete pavement slabs. The

stresses and strains reduce significantly compared to a situation where no load transfer devices are present. Larger diameter dowels provide better load transfer and control of faulting under heavy traffic rather than small diameter dowels. In the analysis several mechanistic approaches were employed to calculate the load transfer efficiency. Strains and Stresses in loading and unloading slabs are factors used to calculate the load transfer efficiency between loading and unloading slabs. Precast repair sections with higher LTE are expected to perform better since lower differential settlements will be present once loads are applied. The load transfer efficiency is calculated using the ratio of maximum deflection at joint of the loaded slab and the deflection of unloaded slab measured across the joints. The concept is reflected in Equation 1 where "d_u" is the plastic deformation under unloaded slab and "d_l" is the plastic deformation under loaded slab. An LTE value of 1 is considered as the optimal performance of the pavement structure, while a 0 is the worst possible performance [10].

$$LTE_{\delta} = \frac{d_u}{d_l} \tag{3}$$

Two particular permanent deformation approaches used to characterize rutting behavior of pavement structures subjected to traffic load are "Layer Rutting" and "System Rutting".
The "System Rutting" model approaches the pavement structure as one entire unit; therefore, the resulted deflection of the whole system is equal to the total plastic deformation. The characterization of the deformation behavior of the pavement structures requires only one set of permanent deformation parameters to be modeled. In the case of the "Layer Rutting" the pavement structure is divided into sub layers; additionally, the plastic deformation is calculated for each layer. The sum of the plastic deformation of each layer is equal to the total deformation at the top of the pavement. The plastic deformation is calculated in each layer as a function of elastic strain in the layer and material parameters for each finite layer. Repeated load permanent deformation tests are used in the lab for determining the material parameters.

The HWD geophones measured the total deformation at the top of the pavement structure regardless of the contribution of each of the layer independently. It is imperative to state that Equation 1 is an approach for calculating LTE using the "System Rutting" model rather than the "Layer Rutting" model [10]. An alternative method to calculate the LTE_{δ} can be done using Equation 4 [9].

$$LTE^*_{\delta} = \frac{2d_u}{d_l + d_u} \tag{4}$$

The relation between the two methods for calculating the load transfer efficiency deflection based can be express in Equation 5.

$$LTE^*_{\delta} = 2\left[1 - \frac{1}{1+\frac{LTE_{\delta}}{100}}\right] \tag{5}$$

The load transfer Efficiency could be calculated based on stress. The stress under the PCC slabs at the

joints is used for the calculations. Equation 6 reflects the ratio of stress used to calculate the stress-base load transfer efficiency.

$$LTE_{\sigma} = \frac{\sigma_u}{\sigma_l} \tag{6}$$

Where "σ_u" is the stress at the joint of the unloaded slab, "σ_l" is the stress at the joint of the loaded slab and LTE_{σ} is the stress-based load transfer efficiency.

4.5 Deformation Energy

The deformation energy concept was employed to characterize the amount of energy dissipated through the subgrade soil. The differential energy concept is defined as the energy difference in the elastic subgrade deformation under the loaded slab (leave) and unloaded slab (approach). Originally developed by Larralde the deformation energy was used to characterize pumping and faulting in rigid pavements [12, 13]. The Differential energy can be written as:

$$DE = E_L - E_{UL} = \frac{1}{2}k(\varepsilon_P)_L^2 - \frac{1}{2}k(\varepsilon_P)_{UL}^2 \tag{8}$$

The dissipate energy is a parameter in the differential energy equation. Energy of elastic deformation is assumed to be proportional to the dissipated energy to the subgrade. The dissipated energy due to deformation of the slab is shown in Equation 3. Where "k" is the modulus of selected subgrade and "ε_p" is the Plastic deformation of the edge of selected slab [14]. Pavement systems with lower differential energy are expected to exhibit better performances in the field.

$$E = \frac{1}{2}k(\varepsilon_P)^2 \tag{9}$$

4.6 Joint Stiffness

Orthogonal movement resistance and stability of the joints are critical parameters influencing the load transfer efficiency. Load transfer efficiency through aggregate interlocking, reinforcement dowels bars, and through foundation support are parts of the joint stiffness analysis.

4.6.1 Load Transfer through Aggregate Interlocking

The load transfer through aggregate interlocking is a function of joint stiffness and is related to the shear capacity of the joints, this according to the new mechanistic empirical pavement design guide (MEPDG) [9]. Load transfer through aggregate interlocking resisting shear forces can be obtained by using Equation 6. The parameter "J_{AGG}" represents the transverse joint stiffness [10].

$$LTE_{AGG} = \frac{100}{1+0.012J_{AGG}^{-0.849}} \tag{10}$$

Transverse joint stiffness is a function of shear capacity of the aggregate particles. Aggregate geometry and particle size distribution in the mix. Aggregate geometry refers the aggregate angularity, texture, and form of the particles. Angularity is any broken edges at the corners of the aggregate particles, texture represent the porosity or small asperities at the surface of the particles, and form of particles refers to the shape that the aggregate has. The geometry and the particle size distribution play a crucial role in the LTE_{AGG}. Aggregate particles have better interlocking when the particles are very angular, when the textures are rougher and when they are flat and elongated; better aggregate particles interlocking represent better performance in terms of orthogonal load bearing capacity. Shear capacity and joint stiffness relation can be seen in Equation 7, according to MEPDG [10].

$$Log(J_{AGG}) = -28.4\, e^{-0.35^{-\left[\frac{S-0.35}{0.38}\right]}} \tag{11}$$

Where "S" is shear capacity of the joint at the first loading interval. Shear capacity of the joint can be calculated using Equation 8.

$$S = 0.05 h_{pcc}\, e^{0.032 jw} \tag{12}$$

Where "h_{pcc}" is thickness of the concrete and "jw" is joint spacing.

4.6.2 Load Transfer through Dowels Bars

The load transfer through dowels bars can be determined using Equation 9.

$$LTE_{DOWEL} = \frac{100}{1+0.012 J_d^{-0.849}} \tag{13}$$

Where "J_d" represents the non-dimensional dowel stiffness and can be calculated using Equation 10 and 11.

$$J_d = J_d^* + (J_0 - J_d^*)\exp(-DAM_{DOWEL}) \tag{14}$$

$$J_0 = \frac{120 d^2}{h_{pcc}} \tag{15}$$

Where "J_0"is initial dowel stiffness, "J^*_d" is critical dowel stiffness, "d" is dowel diameter (in) and "h_{pcc}" is the thickness of the concrete slab (in). The critical dowel stiffness (J^*_d) can be calculated with Equation 12.

$$J_d^* = Min\left\{118, Max\left[165\frac{d^2}{h_{pcc}} - 19.8120, 0.4\right]\right\} \tag{16}$$

4.6.3 Load Transfer through Foundation Support

The load transfer through foundation support is obtain by using values presented in tables from the new mechanistic MEPDG [10]. Table 8 presents the suggested Load transfer efficiency values for three different scenarios.

Table 8. Foundation Load Transfer Suggested values for Different Foundation Type

Foundation Type	LTE Foundation
Unbound Aggregate Base	20%
Cement Treated or Asphalt Treated Base	30%
Lime Treated Base	40%

4.6.4 Total Load Transfer Efficiency for Joint Stiffness

All permutations of the experiment were constructed on the same base and subgrade; therefore, the parameter of load transfer efficiency through foundation support ($LTE_{foundation}$) was ignored in the analysis. Joint stiffness was then assumed to be only a function of aggregate interlocking and load transfer devices (dowel bars). The total load transfer was calculated using Equation 13 [11].

$$LTE_{Total} = 100\left\{1 - \left[1 - \frac{1}{1+log^{-1}\left[\frac{(0.214-0.183\left(\frac{a}{l}\right)-[log(J)+R]}{1.18}\right]}\right]\left[1 - \frac{LTE_{Foundation}}{100}\right]\right\} \quad (17)$$

Where “R” is load transfer provided by steel reinforcement, “J” is load transfer provided by aggregate interlocking, “a” is radius of the load in HWD (in), and “l” is the radius of relative stiffness.

4.7 Heavy Weight Deflectometer and Back-Calculation of Modulus

A Heavy Weight Deflectometer (HWD) is a non-destructive test used to back-calculate the modulus of pavement components including the subgrade. The device is widely used by highway engineers for an evaluation of the structural capacity of pavements layers. The load levels for a HWD device range from 6,500 to 54,000lbf (30-240kN). The plastic deformation resulting from the drop of the load is measured at the two sides of the joints that are being evaluated. A series of sensors known as geophones are place in several radial distances for measuring of the plastic deformation. The back-calculation is then perform by measuring the deflection basin and varying the set of modulus until a match between the computed and measured deflection is obtain. The best match has to be select for a higher accuracy. Figure 19 shows the HWD equipment.

Figure – 19 Heavy Weight Deflectometer [3]

The HWD test is perform near the edges of two concrete slabs connected with mechanism devices such as dowels. One concrete slab corresponds to the existing slab and the other one to the repair section. A load is applied on one slab creating a plastic deformation on both slabs, which is then measure by a series of Geophones placed on top of the surface and spaced 12 inches apart linearly. The plastic deformation is measured in the loaded slab $(\varepsilon_p)_l$ continuing with the deformation in the approaching slab $(\varepsilon_p)_{ul.}$ Figure 20 illustrates the concept behind an HWD test.

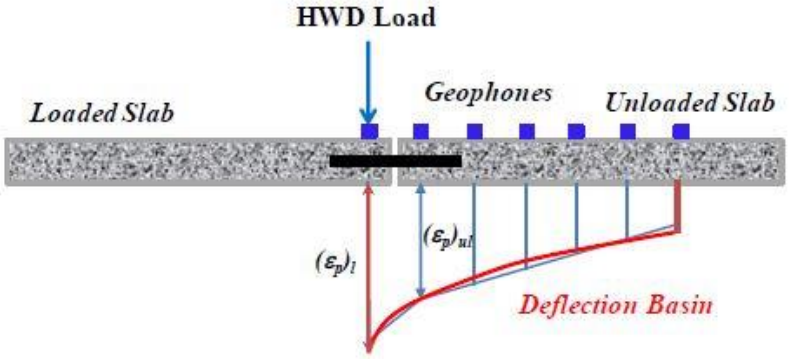

Figure – 20 HWD Test Concept [3]

4.8 Performance Degradation

After a specific time a pavement structure requires rehabilitation. Pavement structures deteriorate from the time of initial serviceability to the time of terminal serviceability; loss of load transfer efficiency and decay in joint stiffness with repetition of load are parameters evaluate to determined the deterioration of pavement structures. The deflection resulting from an application of a HWD test after 0, 112, 256, 512, 752, 1008, 1248 and 1504 impact loads of the F – 15 load cart were measured for this research. The

performance degradation in the repair sections was calculated by monitoring the effects of load application over load transfer efficiency, joint stiffness and deformation energy at each test. The three installation techniques were tested, evaluated, and compared.

The F – 15 load cart carries 35,200 lbs. on a single wheel, approximately a tire pressure is 315 psi. The load represents one-half of the F – 15 aircraft main loading gear. The F – 15 loading cart was used to induce damage by accelerated loading repetition in the repair section for evaluation purposes. Figure 21 illustrated an accelerated loading in a repair section using the F – 15 load cart.

Figure – 21 Loading Cart F-15 [3]

5. Performance Evaluation

The analysis was performed to the three concrete repair panels describe in Section 3. The three scenarios were concrete repair panel #1 installed using HDP foam injection, concrete repair panel #2 installed using HDP foam deep injected three feet into the subgrade, and concrete repair panel #3 installed with flowable fill.

5.1 Back Calculation of the Modulus of Pre-existing Concrete Slab

The evaluation for the existing concrete was performed using a mechanistic approach for the back-calculation of the material properties and the responses were determined using finite element analysis. An HWD test was used to determine the deflection basin under a loading scenario. The deflections measured were in turn used to determine the material properties of each pavement layer. The HWD test was performed at the middle of the slab when back-calculating the modulus of the pre-existing slab. This is done to eliminate back-calculation errors imposed by discontinuities at the joints and boundary conditions in the finite element simulations. Table 9 presents the deflection resulted at the top of the pre-existing concrete slab when the HWD test was performed. The results are in mils units where 1 mil = 0.001 of an inch.

Table 9. Pre-existing Concrete Slab Deformations from HWD test at Mid-slab Loading

Station	*Load (lbs)*	d_1	d_2	d_3	d_4	d_5	d_6	d_7
1	58,331	16.37	15.03	13.26	11.39	9.54	7.73	6.22
2	58,046	17.68	16.22	14.53	12.62	10.56	8.43	6.46
3	58,134	19.57	17.38	15.06	12.66	10.25	7.98	5.98
4	57,729	20.67	19.2	17.7	16.07	14.1	12.07	10.31
5	58,266	18.26	16.59	14.6	12.48	10.26	8.08	6.13
6	57,992	20.03	18.29	16.35	14.31	12.06	9.8	7.68
7	58,397	18.1	16.2	14.01	11.87	9.71	7.72	5.83
8	57,630	19.97	18.02	15.93	13.78	11.57	9.47	7.4
9	58,583	20.18	17.81	15.25	12.85	10.41	8.14	6.24
10	58,309	20.34	18.86	17.2	15.47	13.43	11.48	9.84
11	58,320	19.65	17.45	14.99	12.53	10.13	7.83	5.9
12	58,068	21.04	19.69	18.22	16.61	14.78	12.88	11.15
13	58,145	19.21	16.76	14.39	12.06	9.76	7.69	5.88
14	58,123	19.41	17.72	15.83	13.84	11.76	9.7	7.74
15	58,627	17.41	15.68	13.69	11.63	9.52	7.61	5.99
16	58,266	18.87	17.3	15.45	13.42	11.14	8.94	6.87
Mean		19.17	17.39	15.4	13.35	11.19	9.1	7.23
Standard Deviation		1.3	1.28	1.41	1.58	1.66	1.69	1.73
Coe. of Variation		6.76	7.36	9.18	11.8	14.82	18.62	23.9

A finite element simulation was performed to obtain several plastic deformation values using various ranges for the modulus of elasticity and LTE_x. Subsequently, the modulus of elasticity and LTE_x values best matching the HWD test plastic deformation were selected. An iterative process using the finite element simulations had to be done to obtain the parameters for the existing concrete slab. Table 10 presents the plastic deformation results and the variables used for the finite element simulation.

Table 10. Results and Variables for the Finite Element Simulation

Simulation ID	LTE_x (%)	E_{pcc} (ksi)	FE Calculated ε_p
1-90-1	90	1000	0.0407
2-90-1	90	2000	0.0336
3-90-1	90	3000	0.0381
4-90-1	90	4000	0.0259
5-90-1	90	5000	0.0249
1-95-2	95	1000	0.0403
2-95-2	95	2000	0.0378
3-95-2	95	3000	0.0333
4-95-2	95	4000	0.0256
5-95-2	95	5000	0.0246
1-100-3	100	1000	0.0349
2-100-3	100	2000	0.0320
3-100-3	100	3000	0.0270
4-100-3	100	4000	0.0184
5-100-3	100	5000	0.0172

The deflection basin for the existing concrete slab was determined using the plastic deformation obtained from the HWD test. The strains and stresses were calculated using a finite element approach. The measured surface deflections were in turn compared to the plastic deformation obtained from the finite element method. Figure 22 illustrates the plastic deformation calculated in the surface of the existing concrete slab using a finite element approach. The plastic deformation is for one of the variations in the values for the modulus of elasticity and LTE_x of the experiment design. The deflection was measure in inches.

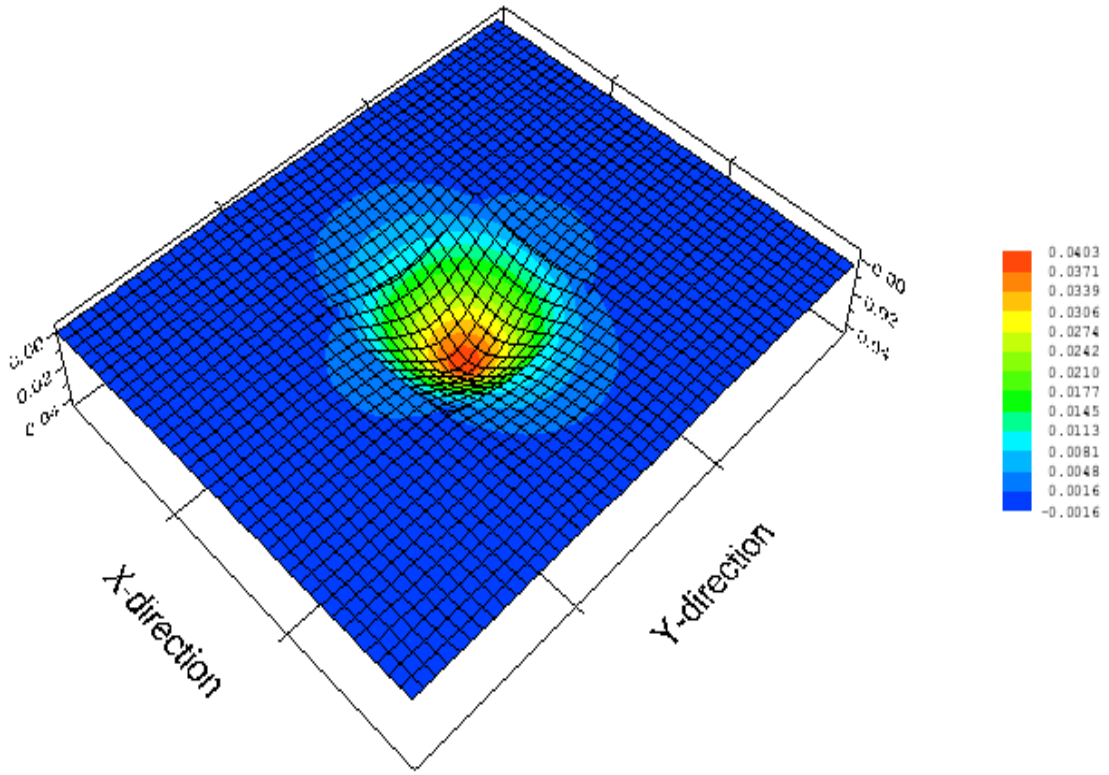

Figure – 22 Deflection Contour Plot for Deformation for E_c=1,000 ksi and LTE_x=90%

Figure 22 represents the contour plot for deformation of the extreme scenario where the concrete modulus of elasticity has a value of 1,000,000 psi and an LTE_x of 90%. The X-direction in the figure represents the direction in which the load transfer devices were installed 12-inches apart of each other and the Y direction was taken as the direction of travel.

5.1.1 Plastic Deformation at the Surface of Concrete Slab

The impact of load transfer efficiency variation was observed when calculating the distresses with the finite element approach. Two contour plots of the plastic deformations at the surface of the concrete were plotted. Both of them had a modulus of elasticity of 4,000 ksi; however, with different values for LTE_x. The reduction of the load transfer efficiency in the X-direction from 100% to 90% implied an increment in the maximum deflection of an estimated 26 percent in the concrete slab. The notable increment in the maximum deflection evidently demonstrates the importance in the variation of the

LTE_x; therefore, the parameter of LTE_x had to be taken as another variable for the experiment analysis. Figure 23 represents the contour plots of the plastic deformation for case (a) having an LTE_x of 100% and case (b) having an LTE_x of 90%.

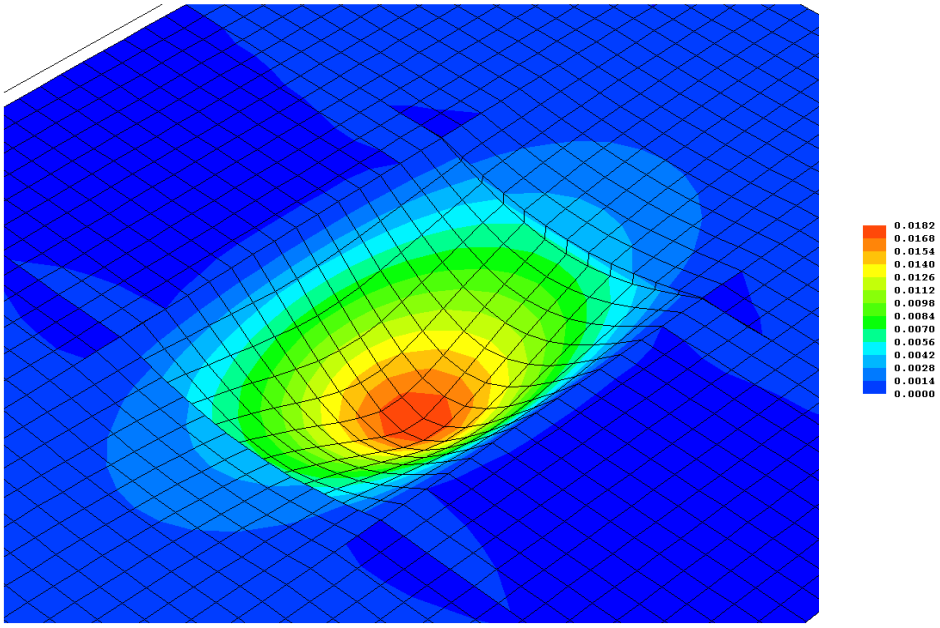

Case (a)

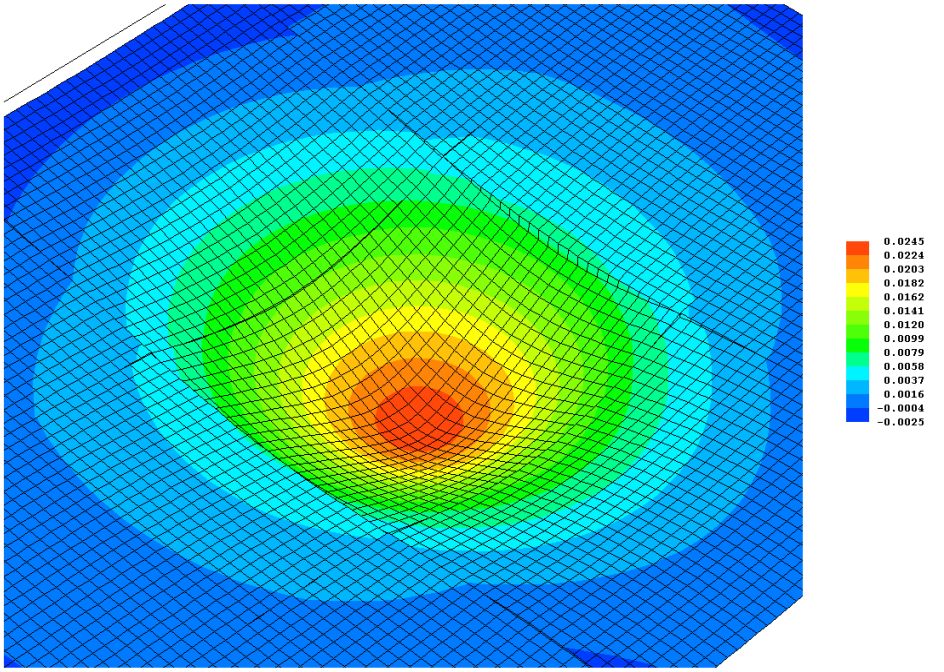

Case (b)

Figure – 23 Contour Plots of the Deflections for the Mid-slab Loading Ec=4000 ksi Case (a) LTE_x=100% and Case (b) LTE_x=90%

5.1.2 Vertical Stresses at the Top of the Subgrade

The distribution of the stresses in the rigid pavement resulted for the finite element analysis was plotted for a visual analysis. The vertical stresses acting at the top of the subgrade were plotted for a concrete slab with a given value for LTE_x of 90 percent and the concrete modulus was assumed to be 5,000,000 psi. The maximum vertical stress took effect at the centerline of the HWD loading system and the stresses were reduced nonlinearly with offsets from load plates. Figure 24 displays the distribution of the stresses.

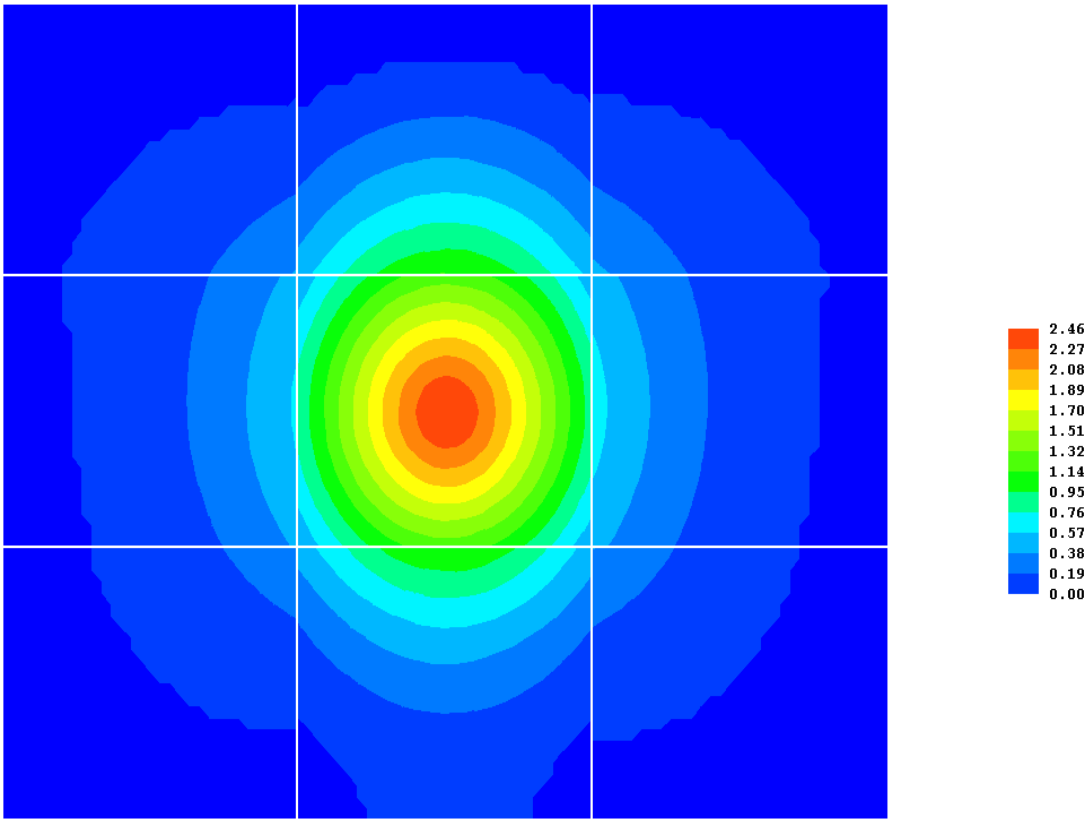

Figure – 24 Distribution of Vertical Stresses at the Top of the Subgrade

LTE_x=90% and E_c=5000 ksi

The contribution of the adjacent slabs and the supporting foundation in the distribution of the stress inflicted by the HWD test is reflected in Figure 24. The distribution of the stress in the approaching slab is not equal to zero; therefore, there is a contribution in the supporting foundation and adjacent slab to handle the stress imposed by the HWD loading system. The distribution of stress illustrated in Figure 24, different patterns are shown in the stress distribution between the direction of travel (Y-direction) and the direction perpendicular to the direction of travel (X-direction). The reason for this behavior is that the load transfer devices were placed in the direction of travel (Y-direction) and the load transfer efficiency in the X-direction was assumed as a constant value along the joints in the X-direction.

5.1.3 Shear Stresses at Top of Concrete and Vertical Stresses at Top of Base Layer

The distribution of shear stresses at the top of concrete slabs and the distribution of vertical stresses at the top of the base layer resulted from a finite element analysis were evaluated separately. The evaluation was performed by plotting the corresponding distress developed on each region of the pavement structure when the HWD test was performed. The LTE_x and modulus of elasticity values were assume as 90 percent and 5,000,000 psi, respectively.

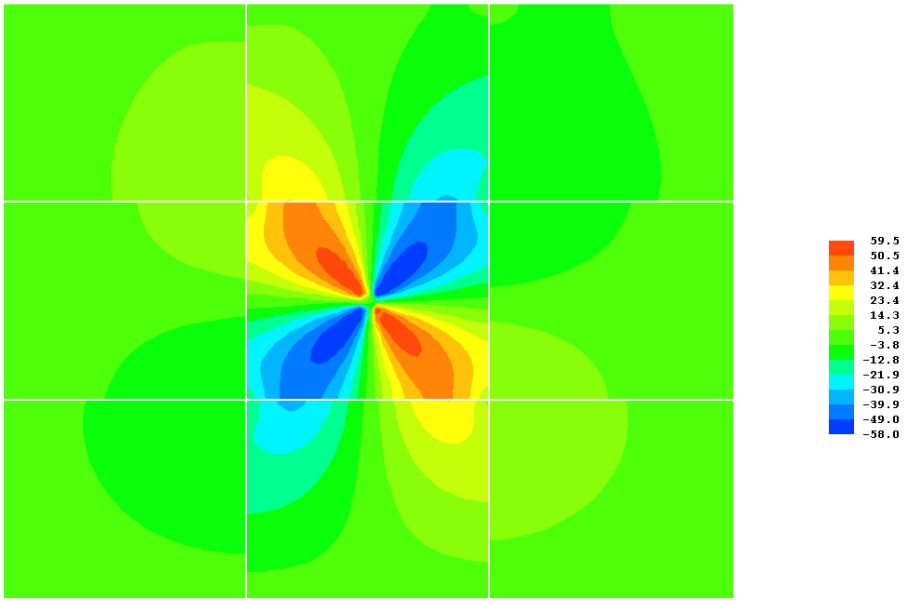

Figure – 25 Shear Stresses at the Top of the Concrete slab, LTE_x=90% and E_c=5000 ksi

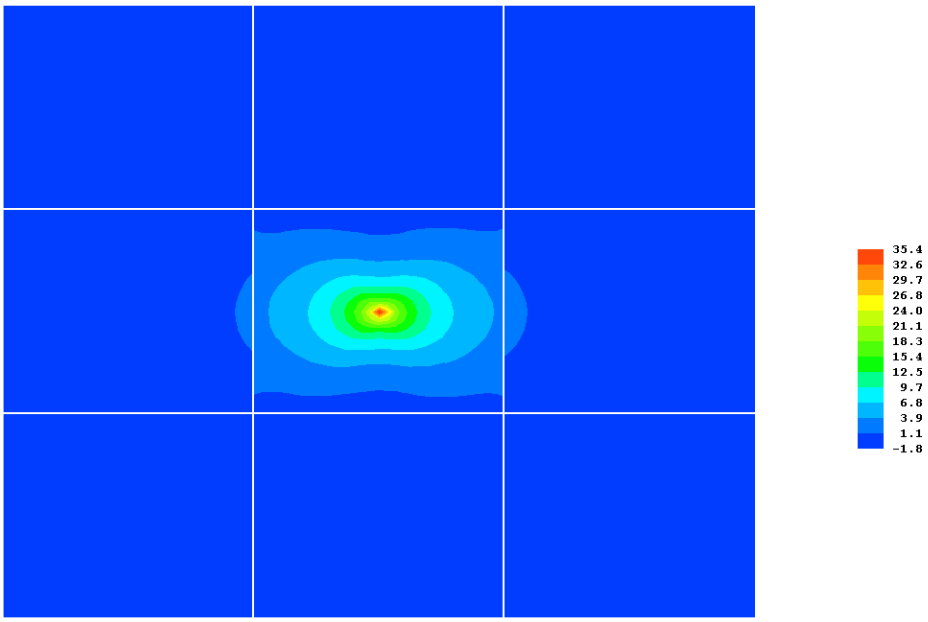

Figure – 26 Vertical Stresses at the Top of the Base Layer, LTE_x=90% and E_c=5000 ksi

The distribution of shear stresses at the top of the concrete shown in Figure 25 resulted to be zero under the load centerline with one side of the load in a compressive state and the other side of the load in a tensile state. The sign of the shear stress depended on the direction of the moving load. The shear stresses increased with distance; however, once reaching the maximum shear stress it started to decrease with respect to distance. Furthermore, The distribution of vertical stresses at the top of the base layer is shown in Figure 26. The difference between the pressures at the direction of travel (Y-direction) and the direction perpendicular to aircraft load (X-direction) are clearly shown the figure. The reason for the differences is the assumptions in the load transfer parameters for the two sides of the slab.

5.2 Analysis of Concrete Repair Slabs

A C-17 Aircraft with a gross weight of 227,707 kg (502 kips) was used for the analysis. The C-17 was selected since it has one of the largest gross weights in transportation industry. A large load results in larger values in the analysis that could better understand. The analysis was performed simulating a C-17 aircraft at loading static conditions. One of the two landing gears arrangements was simulated to be on top of the concrete repair panel. The front and remaining back landing wheels were simulated to be in the existing concrete slab. Figure 27 displays a C-17 aircraft with his landing wheel configuration.

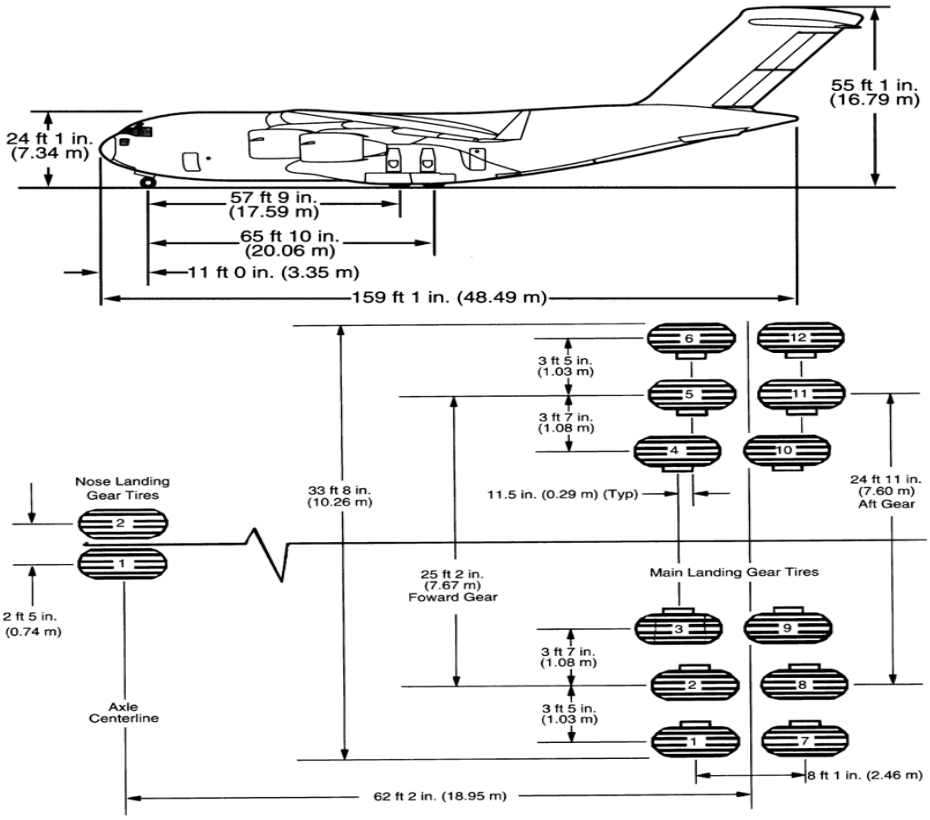

Figure – 27 Wheel Configuration of C – 17 Aircraft [3]

The distresses on concrete slabs under a simulated stationary C-17 landing gear configuration were evaluated. Five different loading positions were evaluated for the repair concrete panel to get the

concrete repair panel scenario with the worst distresses. Figure 28 illustrates the five different scenarios.

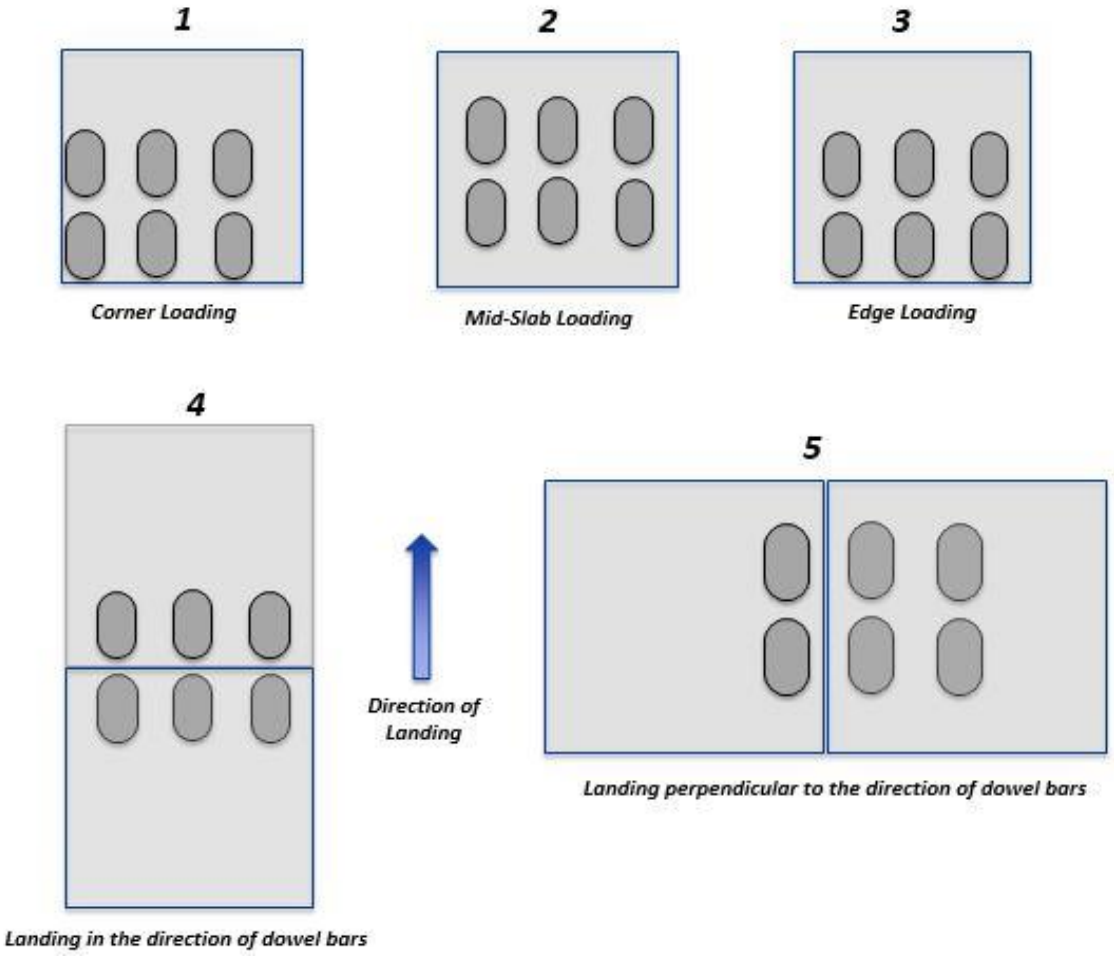

Figure – 28 Scenarios for Loading Position of a C – 17 aircraft [3]

Scenario 2 was not the critical scenario since the load was applied in the middle of the slab and the space to distribute the load was wide and long before it reached an approaching section. Scenarios 4 and 5 were not the critical senario either since the load was distribute between the two slabs directly. The crital scenarios were the number 1 and 3. Corner loading and edge loading were the critical senarios since the load was applied in a position where the load was only handled by one single concrete slab and the area to dissipated the load before reaching the load transfer devices was relative small. Scenarios 1 and 3 were more prone to develop distresses such as edge or corner breakeages in the pavement structure. Edge or corner breaks are cracks that extend vertically through the entire slab thickness cause by load repetition, loss of support, poor load transfer mecanisms and wraping and curling stresses.

5.2.1 Finite Element Analysis

A finite-element analysis for the rigid pavement structure was performed. This analysis is considered more realistic when the base and the sub-base exist above the subgrade and the foundation is considered as a layer system. The analysis simulates the deflection of a concrete slab when an aircraft is

motionless on top of it. The superposition method was used to calculated the distresses for the concrete slabs. Superposition assumes the concrete slab behaves elastically for the combination of loads and the the final distress is the combination of all deflections or stresses cause by each indviaual load.

5.2.1.1 Deformation under Accelerated Loading Conditions

The deformation in the entire concrete slab, existing slab and repair section, was measured and plotted. Figure 29 simulates the deflection cause by a stationary C – 17 aircraft. The static C – 17 aircraft was simulated with the position as the scenario #1 from the loading positions described in Figure 28. This since the corner loading position resulted in the case with the most deformation. Corner loading position in the concrete slab is described in Figure 29. The highlight red square in the left bottom part of the figure is the concrete repair panel positioning six C – 17 aircraft landing wheels in the corners position. The other dots in the figure represent the location of the entire landing gear. The six dots in the bottom right are the parallel six landing wheel of the airplane and the two top dots in the figure are the frontal part of the aircraft.

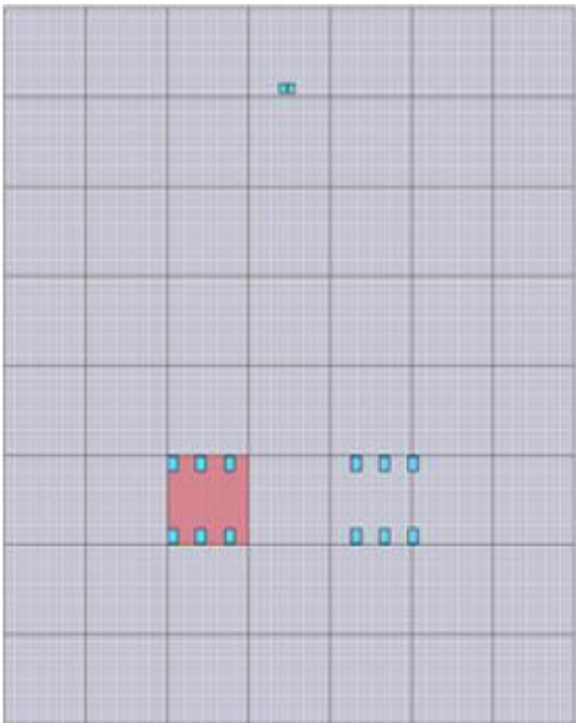

Figure – 29 Corner Loading Position [3]

The maximum deformation occurred where the concrete repair panel was installed. The maximum deformation obtained was 0.0814 in. Notice that the minimum deflection was not zero since the simulation took into account the temperature variations. During daytime the temperature at the top of the slab is greater than at the bottom causing the top part to expand while the bottom tends to contract. The curling concept is shown in this analysis; therefore, the deflection where no loading was applied was 0.041 in. The results for the deformation are shown in Figure 30.

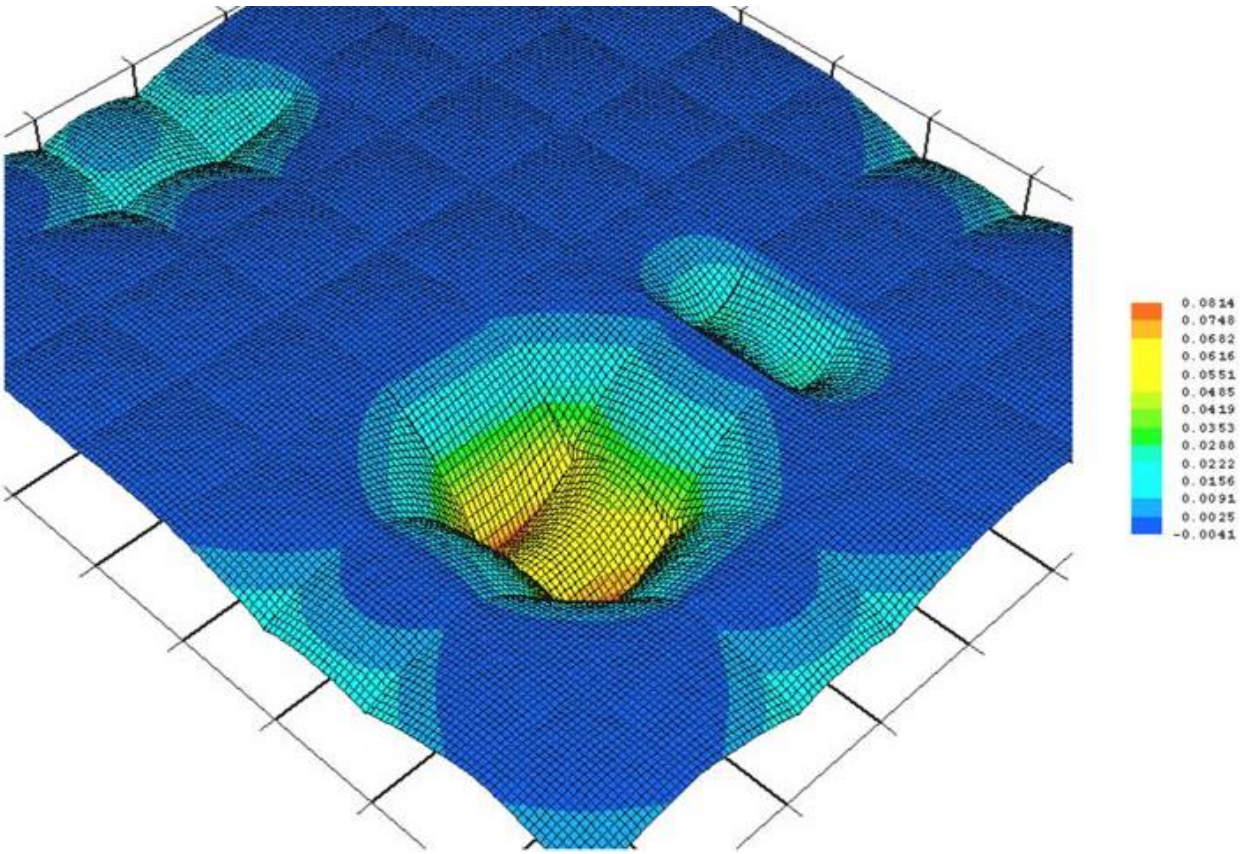

Figure – 30 Deflection cause by C – 17 landing in Panel #1

The maximum plastic deformation for the three slabs under C-17 landing gear were calculated. The three cases were slab #1 which had the base preparation using HDP foam, slab #2 installed using HDP foam deep injected into the subgrade and slab #3 having an installation with flowable fill. The minimum plastic deformation is equal to a preferable performance of a pavement structure. Slab #2 behaved the best since it had the lowest plastic deformation, slab #1 behaved the worst since the plastic deformation was the highest and slab #3 was in-between. The results for the maximum plastic deformation for each slab are shown in Figure 31.

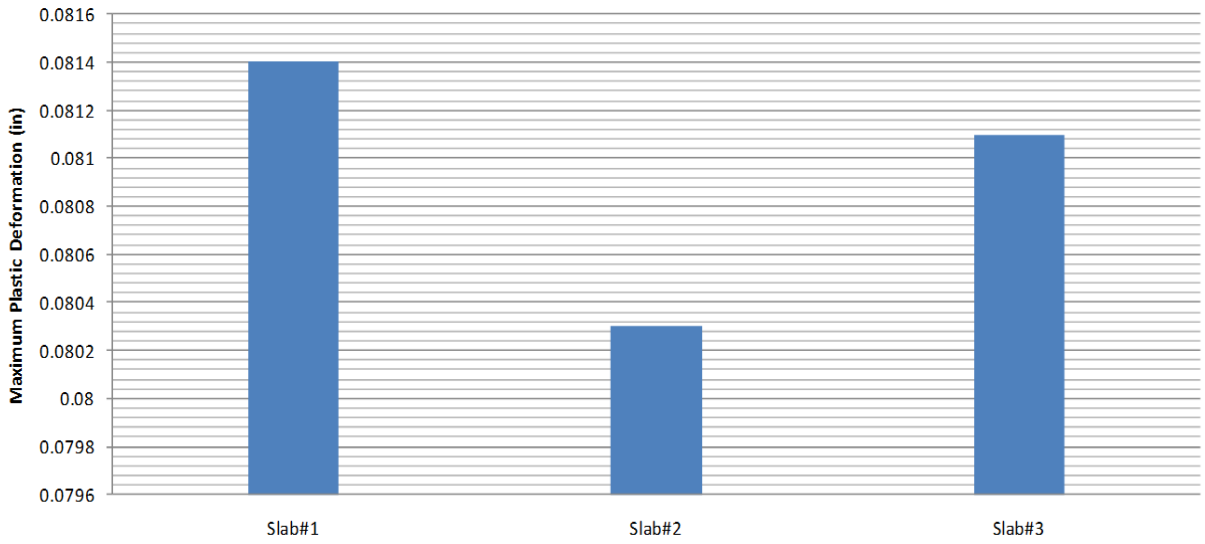

Figure – 31 Maximum Deflections under C – 17 Landing Gear Configurations

5.2.1.2 Vertical Stress under Landing C – 17 Gear Configuration

The results for the vertical stresses at the top of the subgrade for the corner/edge loading scenario in slab #1 are reflected in Figure 32. The simulation of the static aircraft was the same as in the analysis for the deflection. Corner/edge positioning of the load reflected the higher stress inducement into the concrete repair slabs; therefore, it was chosen for the analysis. The higher stresses resulted to 12.20 psi at the location where the concrete repair panel was installed. In this case the minimum possible stress is zero, since the stress discussed in this section is at the top of the subgrade and not in the concrete slab; therefore, the curling and wrapping effect does not apply.

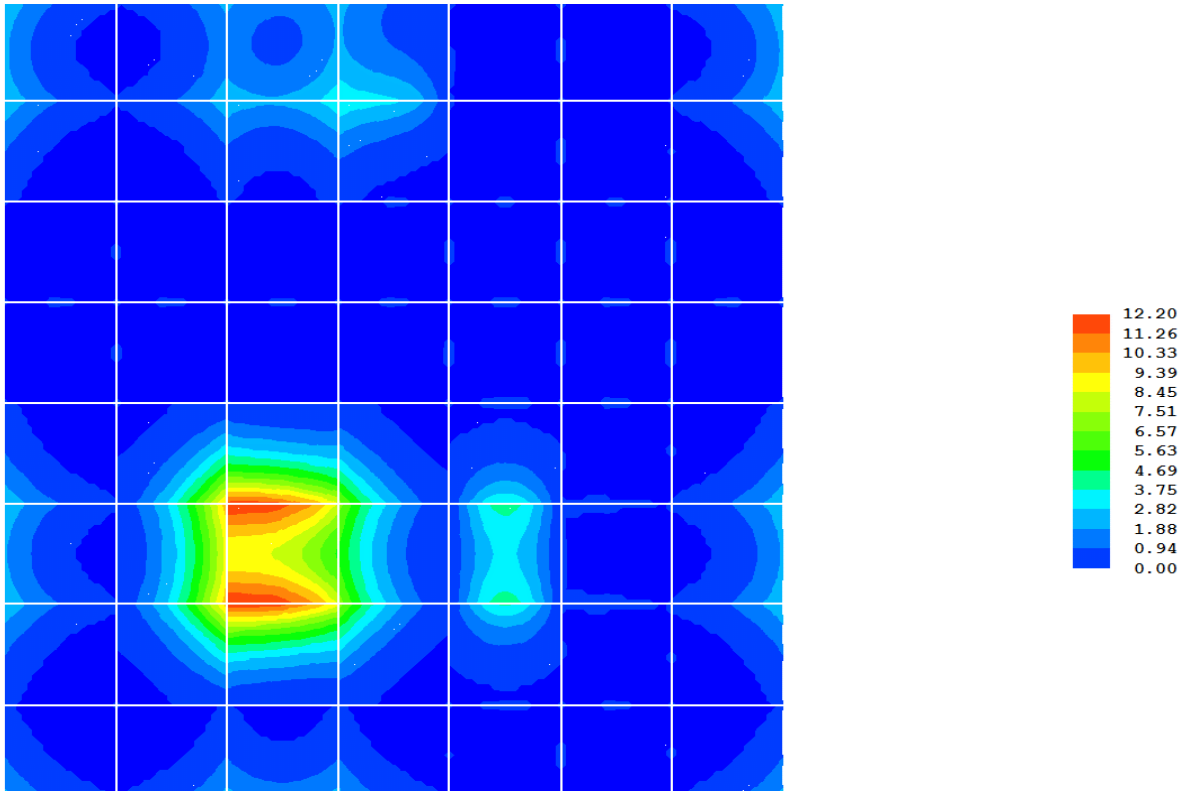

Figure – 32 Distribution of Vertical Stresses at the Top of Subgrade for Slab #1

5.2.2 Measure of Performance

Vertical stress and strength of the concrete are important parameters factors in the design of a pavement. The function of the concrete pavement is to reduce the vertical stress before reaching the top of the subgrade to prevent detrimental pavement deformation. The reduction of the vertical stresses in the concrete pavement depends on the concrete compressive strength; therefore, the design factor was used to evaluate the performance of the concrete repair slab. The three concrete repair panels were evaluated using the design factor criteria.

5.2.2.1 Design Factor (Stress/Strength)

The evaluation of each concrete repair slab (panel) was performed using the design factor criteria stress over strength. The ratios of the maximum vertical stress on concrete ($\sigma_{v\text{-}max}$) over concrete modulus of rupture (S_c) were compared for an evaluation. Pavement systems with lower strength ratio values are expected to perform better and are less prone to develop distresses associated to faulting and corner breakage. The calculation for the concrete modulus of rupture (S_c) was performed using Equations 1 and 2. The concrete compressive strength (f'_c) was calculated from Equation 2 using a modulus of Elasticity (E_c) value of 5,000,000 psi for the three concrete repair slabs. The calculated results for the three concrete repair slabs are presented in Table 11. The results for the maximum deformation and load transfer efficiency in x and y direction for the repair slabs are shown as well.

Table 11. Analysis Results of the Concrete Repair Slabs

	LTE_x	LTE_y	$\sigma_{v\text{- Max (Concrete)}}$	$\sigma_{v\text{- Max (sub)}}$	$\delta_{max\ (sub)}$	E_c	f'_c	S_c	SR
Slab#1	82.29	94.54	330	12.2	0.0814	5,000,000	7695	570	0.5788
Slab#2	82.39	97.78	325	12.05	0.0803	5,000,000	7695	570	0.5700
Slab#3	82.49	94.91	328	12.16	0.0811	5,000,000	7695	570	0.5753

An equivalent value for the concrete modulus of rupture (S_c) was obtained for the three slabs since the concrete repair panels were assumed to have the same modulus of elasticity. Maximum vertical stress at the concrete and the concrete modulus of rupture (S_c) parameters were used to get the design factor (SR). The Slab #2 had the lowest Design Factor, Slab #1 the highest and Slab #3 was in between. The design factor criteria states that the lowest the value the more possibilities for a favorable performance; therefore, the installation technique for slab #2 resulted in a more efficient. The design factors for the three slabs are illustrated in Figure 33.

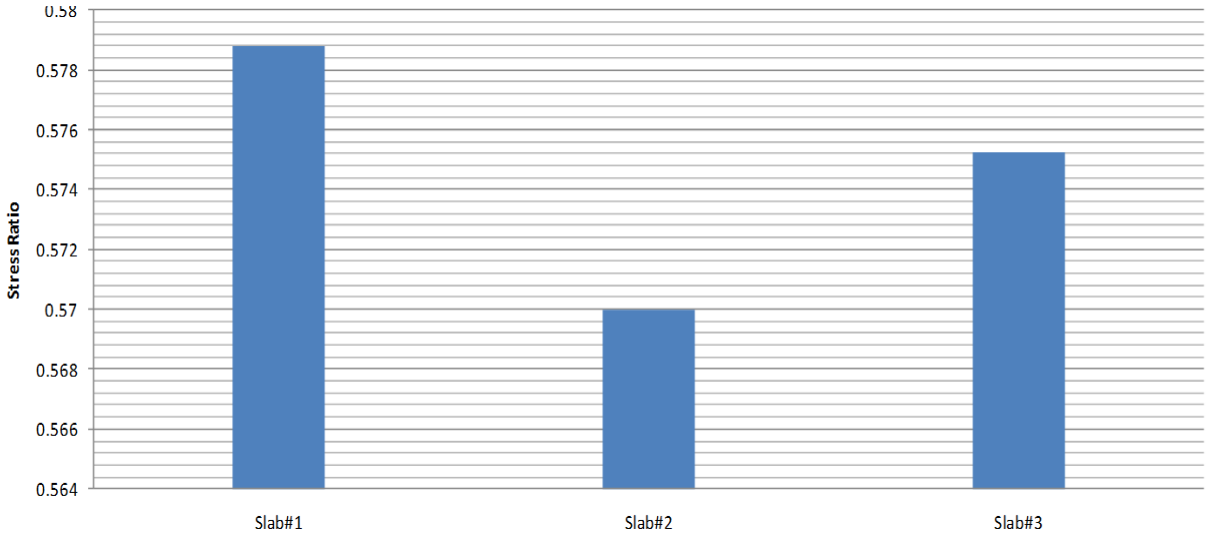

Figure – 33 Design Factor (Max Vertical Stress at Concrete/Concrete Strength

5.2.3 Load Transfer Efficiency (LTE) Analyses

The effects of temperatures variations, aging and accumulation of load repetition in the concrete repair panels are evaluated in this section. The evaluation of the concrete repair panels was performed with a Heavy Weight Deflectometer (HWD) test. The HWD was used to induce a non-recoverable plastic deformation at the joints and the deflections were measured at several radial distances form the impact load. Load transfer was in turn determined at each loading interval to capture the environmental effects and load repetition on the loss of load transfer for different variations of the experiment design. The HWD test drop sequence is illustrated in Figure 34 where the circles are the location where the HWD load was drop. The non-recoverable plastic deformation was measured at two sides of the joints. In other words, the HWD was placed at each side of the joints and the load transfer efficiencies between both slabs, the repair and existing concrete slab, were calculated. Appendix A describes in detail the times, temperatures and dropping sequences for the HWD test application in the three repair slabs.

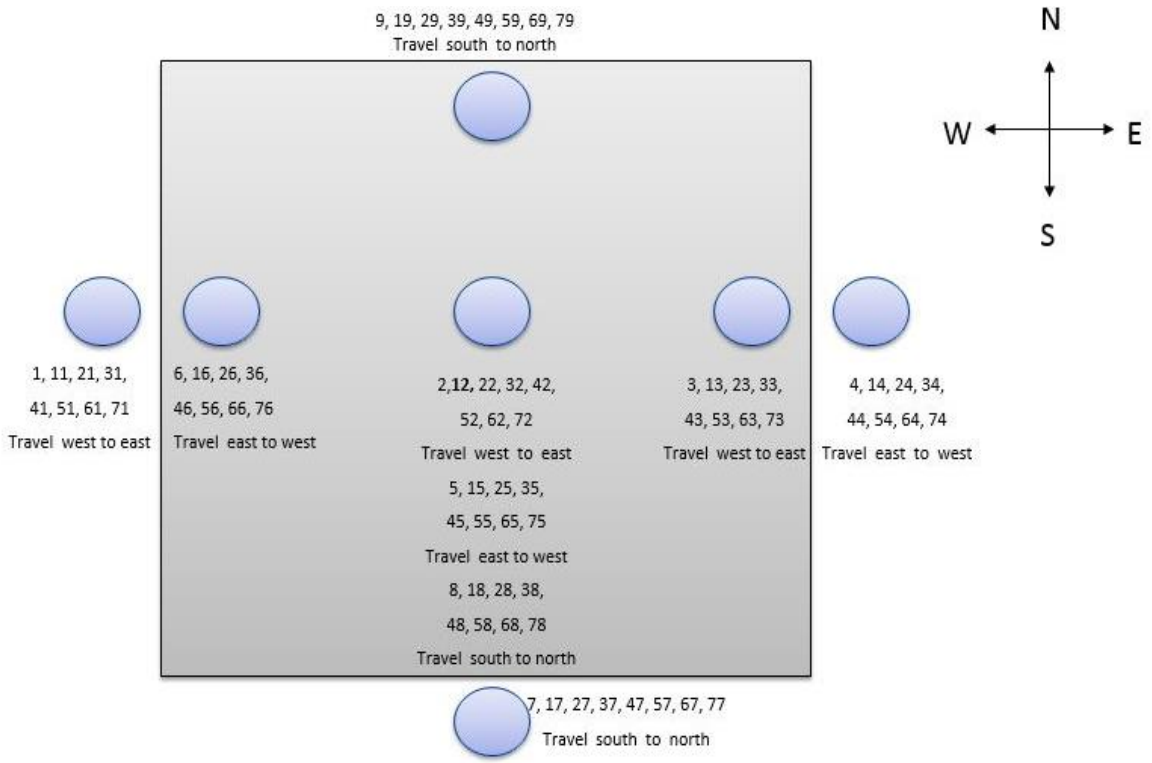

Figure – 34 HWD Test Drop Sequence

Three scenarios for each concrete repair slab where tested and compared for their performance with their LTE. The three scenarios were a concrete repair slab with zero load application, a concrete repair slab with 1504 load applications, and the third one a concrete repair slab exposed for 2 years to environmental effects without any load application. The two first scenarios were tested after the 28-days period for properly curing of the concrete and the temperature distresses were neglected. The accelerated loading was performed using the F – 15 load cart previously described in section 4.8.

5.2.3.1 Joint Stiffness Analysis

The analysis of joint stiffness was performed and reported in the Practice Protocol for Repair Damaged Runways using Precast Concrete Slabs done by AFRL and AFCESA [3]. Load repetition played a critical role in the rigid pavement structures performance; therefore, the analysis is reviewed in this report. Load transfer efficiency through aggregate interlocking, reinforcement dowels bars and through foundation support were evaluated together as part of the joint stiffness analysis. The joint stiffness analysis was performed using Equation 17 describe in section 4.6.4.The load transfer efficiency through aggregate interlocking, reinforcement dowels bars and foundations support is described in Equation 17; however, since all permutations of the experiment were constructed on the same base and subgrade, the parameter of load transfer efficiency through foundation support ($LTE_{foundation}$) was ignored. Joint stiffness was then assumed to be only a function of aggregate interlocking and load transfer devices (dowel bars). A joint stiffness analysis was performed for the three installations technique applying HWD test at different sides of the concrete slabs and with different directions in the travel of load. The joints stiffness of the repair slabs was evaluated with no load application and after 1504 loads application of

an F – 15 load cart. The results shown in figure 35 describe the analysis for initial joint stiffness and for the joint stiffness after 1504 load applications without the consideration of thermal stresses. The equation used in the analysis is also shown in the figure. The results show that slab #2 installed with HDP deep injection performed better than all the rest after 1504 loads application. The decrease in load transfer efficiency before and after the 1504 load application was not as notable in Slab #2 as in the rest of the slabs; therefore, slab #2 outperformed the rest of the slabs tested.

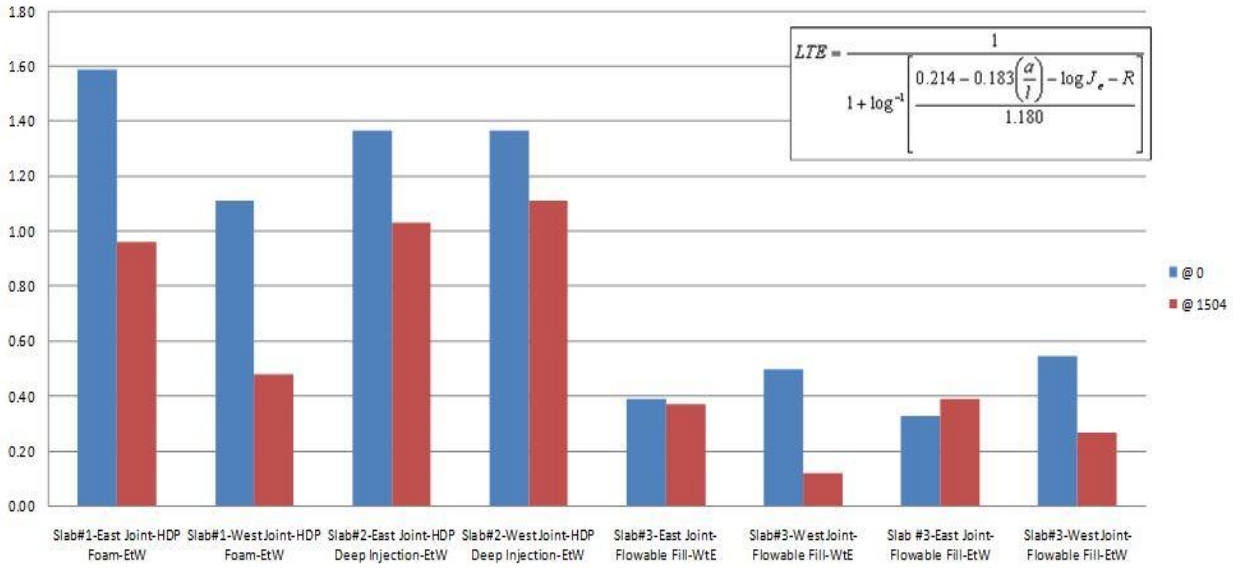

Figure – 35 Initial Joint Stiffness vs Terminal Joint Stiffness

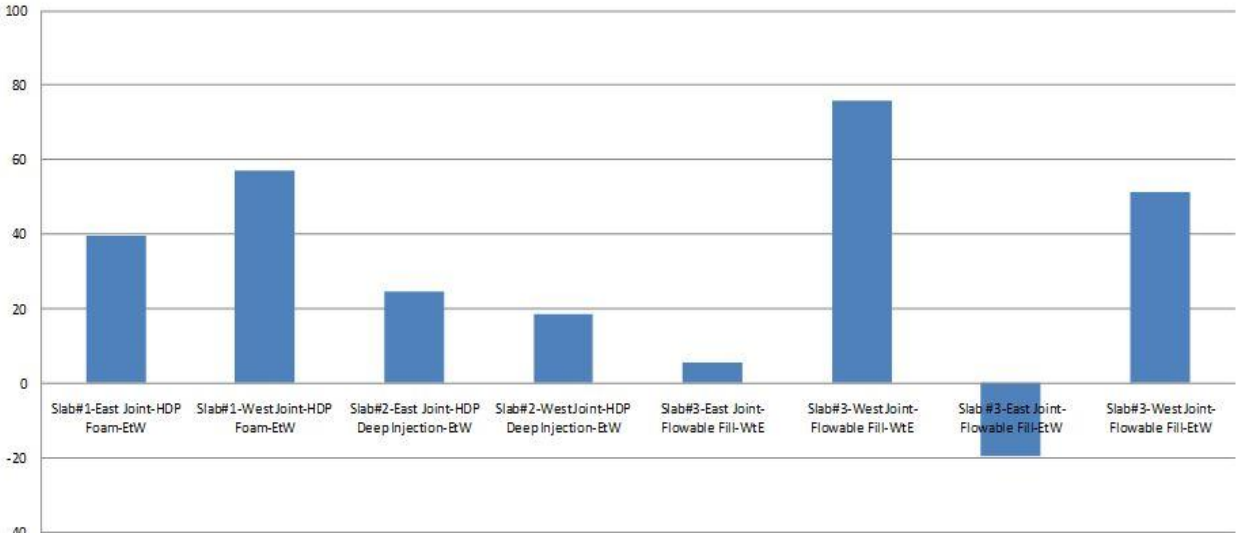

Figure – 36 Loss of Joint Stiffness After 1504 load Applications

The percentage loss of joint stiffness cause by the 1504 load application is shown in Figure 36. Minor losses of joint stiffness are reflected to be in the slabs installed with HDP deep injection and with HDP

conventional installation. The gradient of loss of stiffness is significantly smaller lower for slab #2 and #1; therefore, they had a better performance than slab #3.

5.2.3.2 LTE_{δ}, Neglecting Temperature Distresses only Load Accumulation Analysis

An HWD test was performed to obtain the LTE based on deflection (LTE_{δ}) without considering the temperature distresses in the analysis. The LTE_{δ} was measured directly from the plastic deformation caused by the HWD test. The HWD was placed at each side of the joints and the plastic deformations were recorded for each scenario. The plastic deformations were recorded after 0, 112, 256, 512, 752, 1008, 1248 and 1504 applications of an F – 15 load cart. Subsequently, the LTE_{δ} for each case was calculated and a graph was created to represent the trends of the LTE_{δ} for several scenarios. Equation 3 describe in Section 4.4 was used to calculate the LTE_{δ} for each variation in scenarios and loading intervals. Figure 37 illustrates eight different scenarios in which the LTE_{δ} was determined for the three slabs installed. The LTE_{δ} exact values are available in Appendix A for the eight scenarios. Another set of deflection-based load transfer efficiencies (LTE*) values were calculated using Equation 5 for comparison purpose. The performance trends were similar as when Equation 3 was used. Slab #2 still performed better than the rest of the slabs. The results are available in Appendix A.

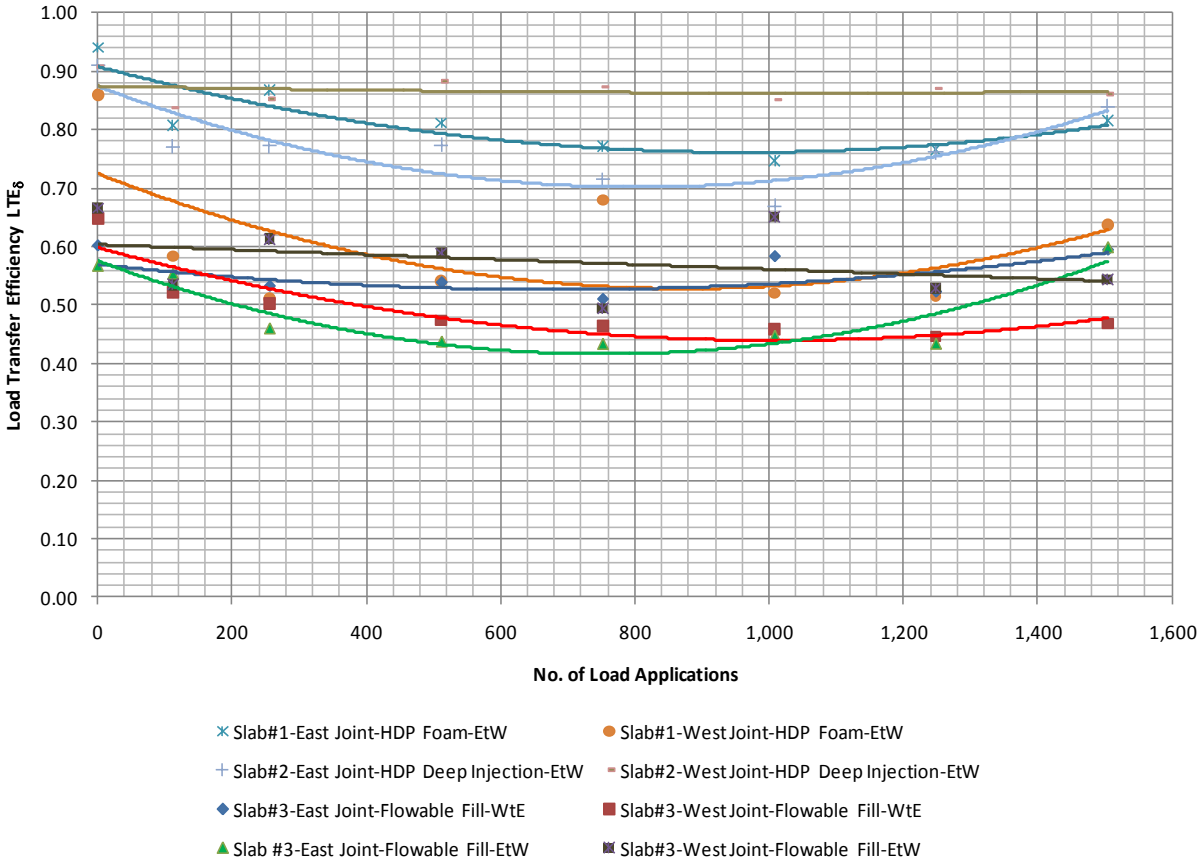

Figure – 37 LTE_{δ} Neglecting Temperature Variation Distresses

5.2.3.3 LTEσ, Neglecting Temperature Distresses only Load Accumulation Analysis

Load Transfer based on stress was analyzed only for accumulation of load applications. The analysis was previously performed and reported in the Practice Protocol for Repair Damaged Runways using Precast Concrete Slabs done by AFRL and AFCESA [3]. Figure 38 displays the results for LTE_{σ} applying a regression analysis for a better understanding of load accumulation. The LTE_{σ} was calculated using Equation 6.

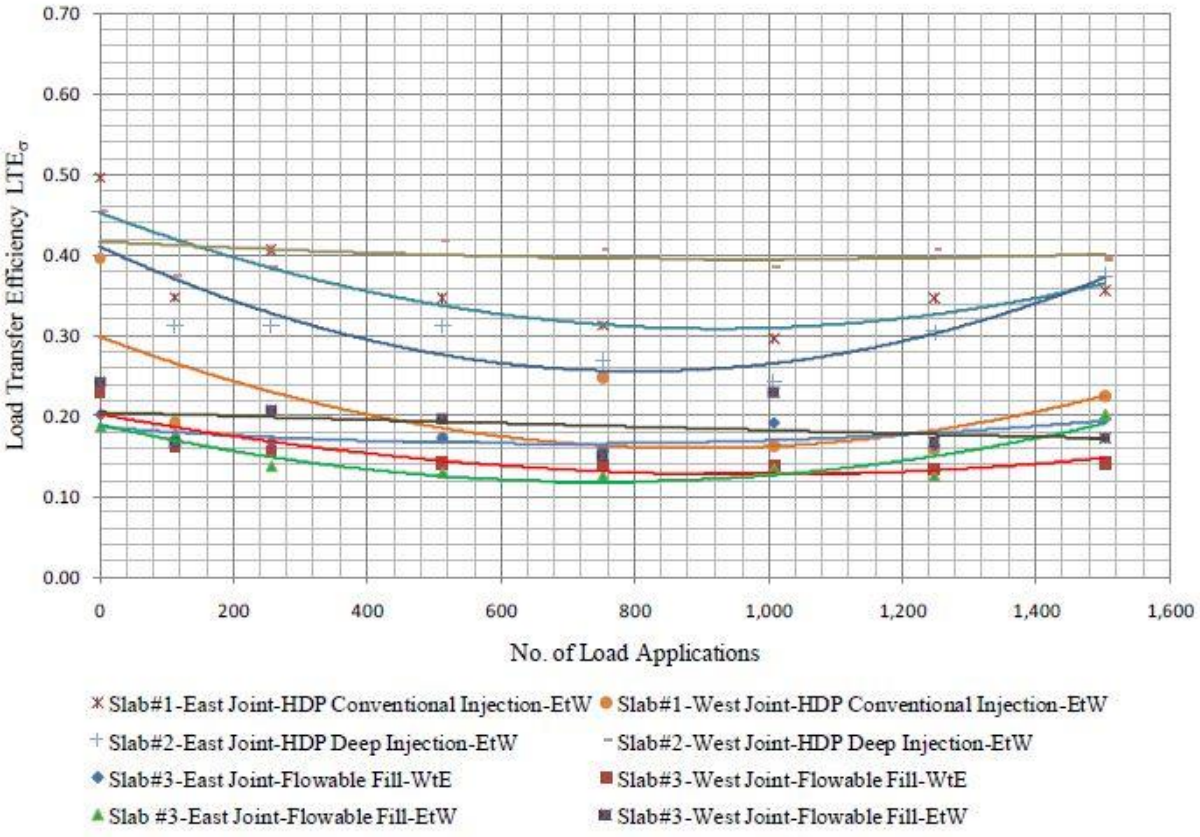

Figure – 38 LTEσ Neglecting Temperature Variation Distress

Slab #2 surpassed both slab #1 and #3 in obtaining higher LTEσ values. Slab #2 obtained higher values for LTE_{σ} than slab #1 and #2 consistently throughout the analysis. Slab #3 installed with flowable fill obtained the lowest load transfer efficiency and slab #1 was in between. Higher values of Load transfer efficiency in concrete repair sections are expected to perform better in terms of orthogonal load bearing capacity; therefore, the application of HDP in the installation procedure of the concrete repair panels resulted in a better performance than flowable fill. No one to one relation exists between LTEσ analyzed in this section and the LTE_{δ} analyzed in Section 5.2.3.2. Although, both LTEs were analyzed in the same circumstances the values for LTEσ ranged from 0.6 for ideal load transfer efficiency to 0 for the worst possible and the values for LTE_{δ} Ranged from 0 to 1. The exact results of the LTEs for the 8 scenarios are display in Appendix A.

5.2.3.4 Concrete Repair Panels Temperatures

The effects of temperature variation throughout the daytime in the concrete repair slabs were evaluated. HWD test applications to calculate the LTE_{δ} of each slab were performed in a time range starting around 6:00 am and finishing around 5:00 pm. The concrete temperatures were monitored with a thermocouple at different locations of the concrete repair panels (slabs). The surface of the concrete, the layer below the grade and at the top, middle and bottom of the concrete slab sections of the pavement structure were monitored. The temperatures at different times of the days were measured for each section. Figures 39, 40, and 41 represent the temperature variations of slabs #1, slab #2 and slab #3 respectively.

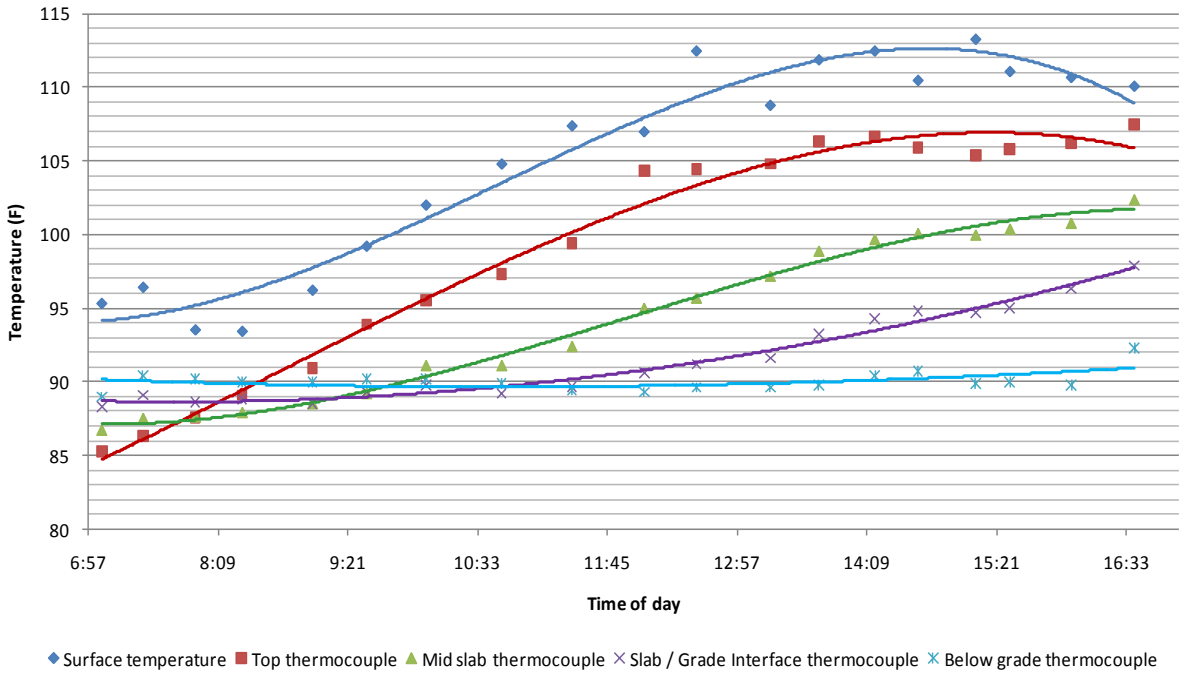

Figure – 39 Slab #1 Temperature Variations vs Time

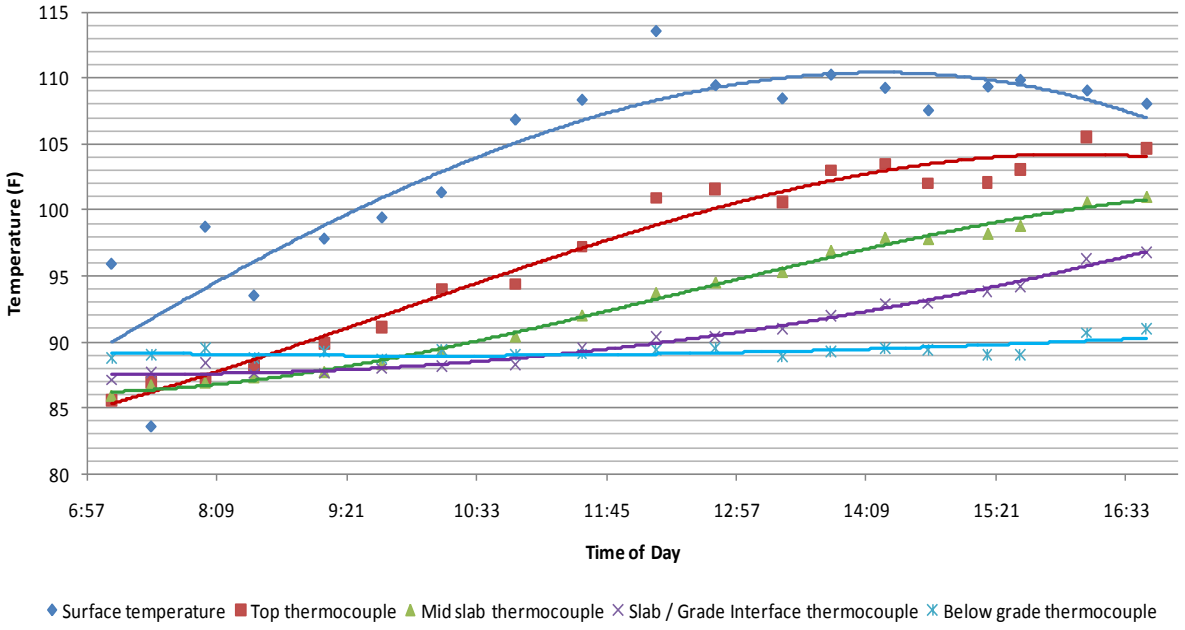

Figure – 40 Slab #2 Temperature Variations vs Time

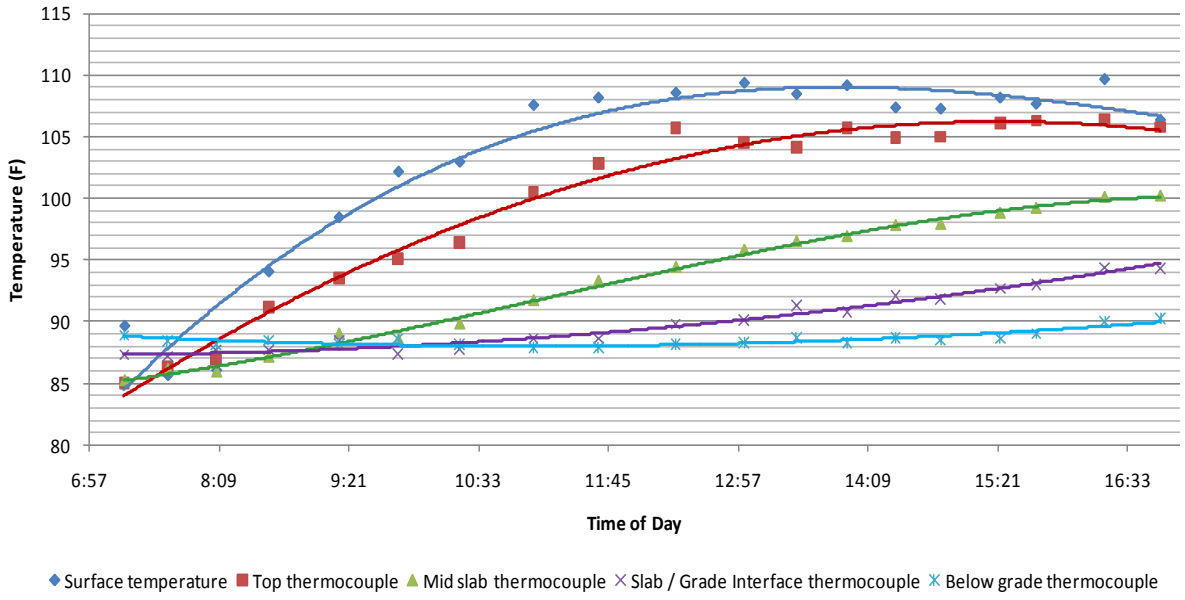

Figure – 41 Slab #3 Temperature Variations vs Time

5.2.3.5 LTE_{δ}, Considering only the Temperature Distresses Accumulations

Three concrete repair panels with no load application on them were installed and aged for 2 years. Accumulations of distresses cause by temperature variation for a period of 2 years were the parameters to evaluate in this section. Slab #1 was installed with HDP foam conventional injected, Slab #2 with HDP foam deep injected and Slab #3 using the flowable fill conventional installation. Curling and wrapping stresses and other environmental factors such as change in humidity were the source of deterioration in the precast repair panel performance.

The deflection resulted from the application of the HWD impact load after 0, 112, 256, 512, 752, 1008, 1248 and 1504 applications of an F – 15 load cart were recorded and plotted for slab #1, slab #2 and slab #3. The variant on each slab tested was the joint location, the load application location, and the positioning of the sensors for calculating the deflection. Figure 34 in Section 5.2.3 can be used to describe the variation of each slab test. The plots representing the LTE_{δ} calculations are shown in Figures 42, 43, 44 for slab #1, slab #2 and slab #3 respectively.

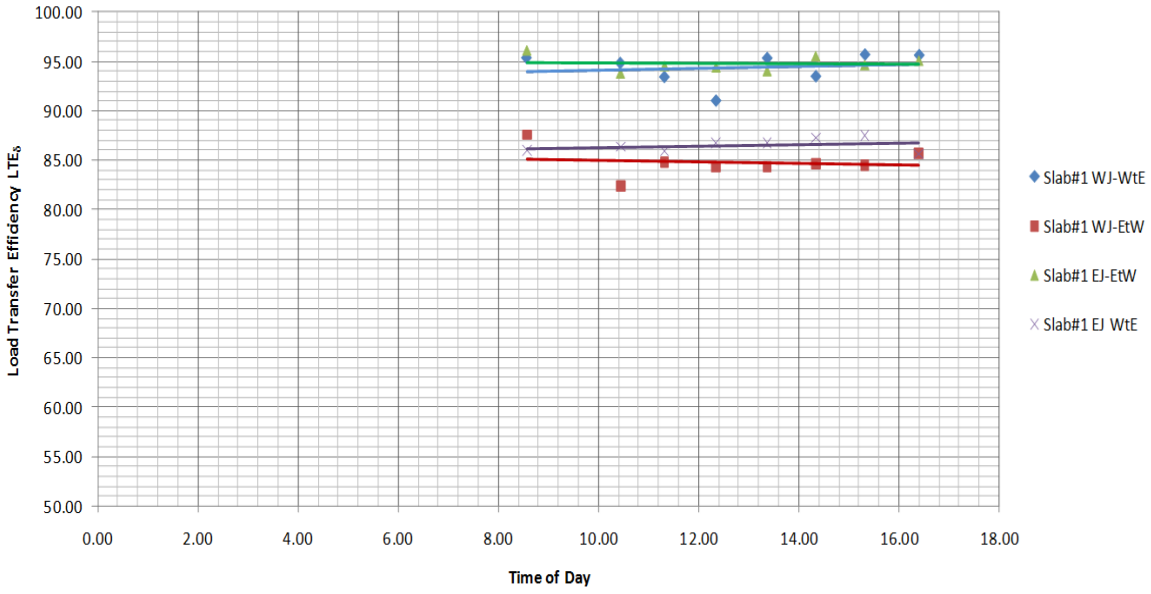

Figure – 42 LTE_{δ} vs Temperature of Time of Day for Slab #1

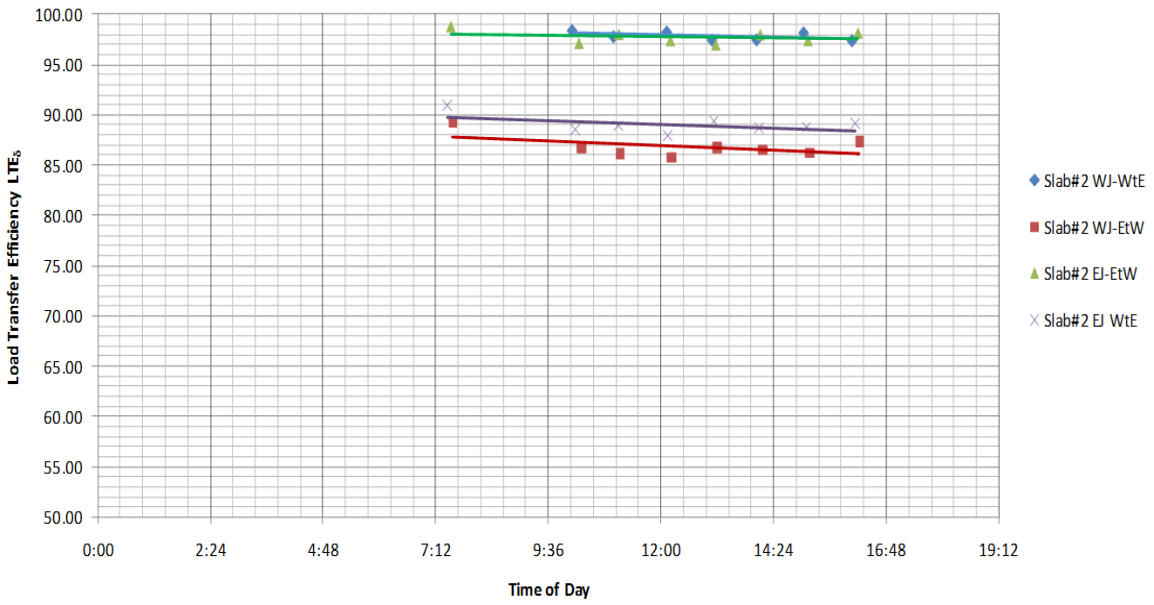

Figure – 43 LTE$_\delta$ vs Temperature of Time of Day for Slab #2

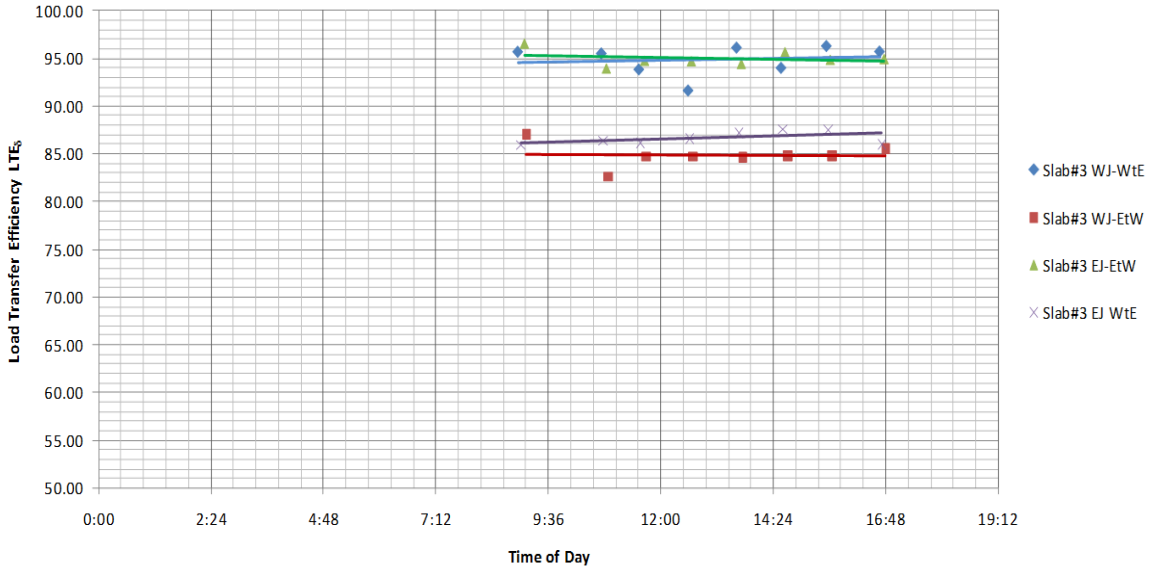

Figure – 44 LTE$_\delta$ vs Temperature of Time of Day for Slab #3

The three slabs behaved more efficiently when the load was measured traveling from the existing concrete to the concrete repair panel. The best scenarios were if the joints were installed in the west boundary of the repair slabs and the deflection was measured from west to east or if the joints were installed on the east boundary of the repair slabs and the deflection was measured from east to west. The worst scenarios were when the load was measured traveling from the concrete repair panel to the existing concrete slab.

5.2.3.6 Comparison for the Analyses of LTE Deflection Based (LTE_δ)

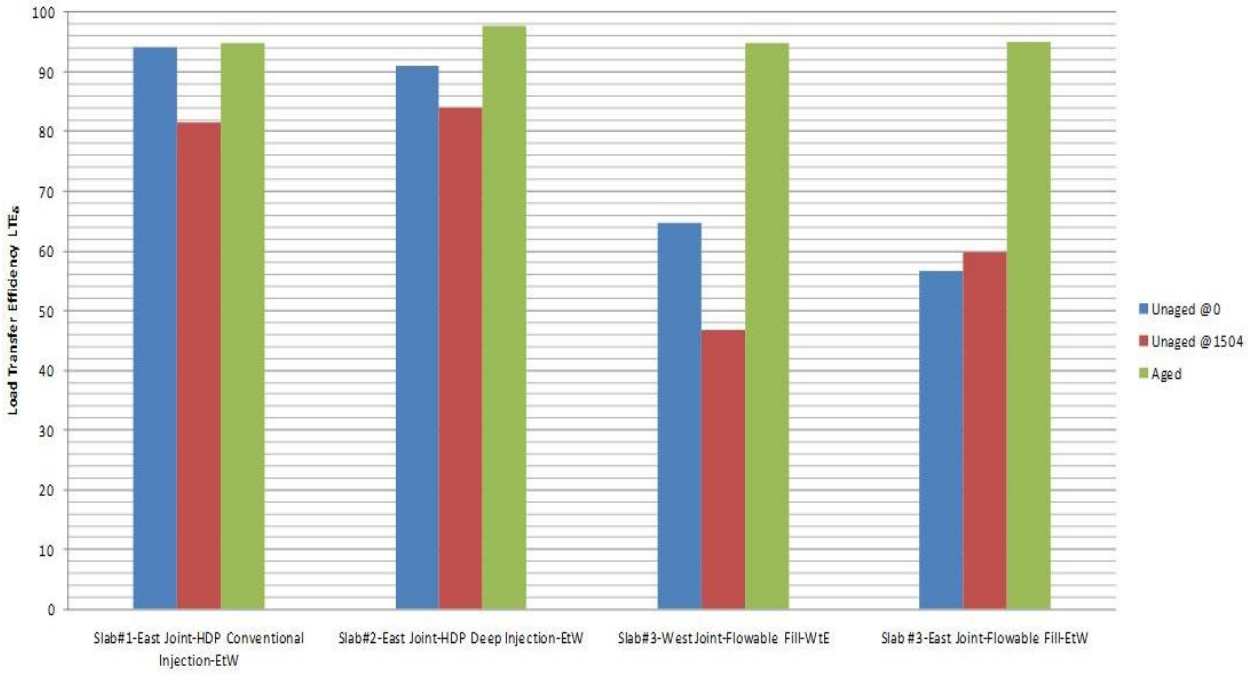

Figure – 45 Comparison of Deflection Based LTE

Table 12. Results for Deflection Based LTE_δ

	LTE_δ		
	Unaged @0	***Unaged @1504***	***Aged***
Slab#1-East Joint-HDP Conventional Injection-EtW	94	82	95
Slab#2-East Joint-HDP Deep Injection-EtW	91	84	98
Slab#3-West Joint-Flowable Fill-WtE	65	47	95
Slab #3-East Joint-Flowable Fill-EtW	57	60	95

Load transfer at the east joint of slab #1 and #2 resulted with the highest values for load transfer efficiency. The performances for both slabs were satisfactory; however, slab #2 outperformed slab#1. The reduction of load transfer efficiency with accumulation of load repetitions was larger in slab #1 than in slab #2. Slab #2 reduction of load transfer efficiency was of 7% and reduction of load transfer efficiency for slab #1 was 12%. These reductions in the load transfer efficiency were caused mainly by the accumulation of load applications. The slab #3, installed with flowable fill, was found to perform worst compared to the other design variants; the results are shown in Figure 45. The results show that the load transfer efficiency for the slab #2 was higher in compare to the other design variants for the no load application analysis. The concrete repair panels were exposed to the environmental effects for a period of two years and then their LTE_δ were measured. Slab #1 and the two cases for slab #3 resulted with an equal 95% LTE_δ. The LTE_δ for slab #2 resulted 3% higher than slab #1 and #3. Table 12 displays the results.

5.2.4 Deformation Energy

The comparison among the three installation techniques for the amount of energy dissipated through their subgrade soil was another method for evaluation. The dissipated energy was calculated based on the HWD deformations on the loaded and unloaded slabs. Equation 8 and Equation 9 were employed to obtain the deformation energy. The deformation energy for each installation technique was plotted and compared using a radar charts for an acquired valuation of the interaction between multivariate data. Radar charts are two-dimensional chart type designed to plot one or more series of values over multiple common variables by providing an axis for each variables. Values are plotted and then connected with lines creating polygonal shape. The polygonal shape area for each test is then the representation either of an adequate or a poor performance for each data evaluated. In this case smaller area for the polygonal shape represent a lower differential energy; therefore, a better performance.

5.2.4.1 Analysis of Deformation Energies without Considering the Influence of Temperature Gradient

The three concrete repair installation techniques were analyzed as well in a just-installed state. Just-installed state meaning the analysis was done right after installation and curing of the pavement structure before subjecting to climatic distresses. The analysis was performed by the method of comparing the deflection energy calculated for each installation technique. The analysis was performed through obtaining the deflection cause by an HWD test measured after 0, 112, 256, 512, 752, 1008, 1248 and 1504 applications of the F – 15 load cart. Once the deflections were measured, the deformation energies were calculated using the formulas in Section 4.4. This analysis was performed previously and reported in a practice protocol for repair of damaged precast concrete slabs done by AFRL and AFCESA [3]. The relationship between the calculated deformation energy and load repetitions is the focus of this section of the analysis.

The deformation energies for eight different cases were calculated and plotted as represented in the following figures. The radar chart assigned an axis for each of the deformation energy calculated after 0, 112, 256, 512, 752, 1008, 1248 and 1504 applications of the F – 15 load cart. A line connecting each of the deformation energy dots was plotted to create a polygon for each one of the eight cases. Figure 46 shows the radar chart with eight different cases evaluated. The conditions for each one of the eight cases are best describe in Figure 34.

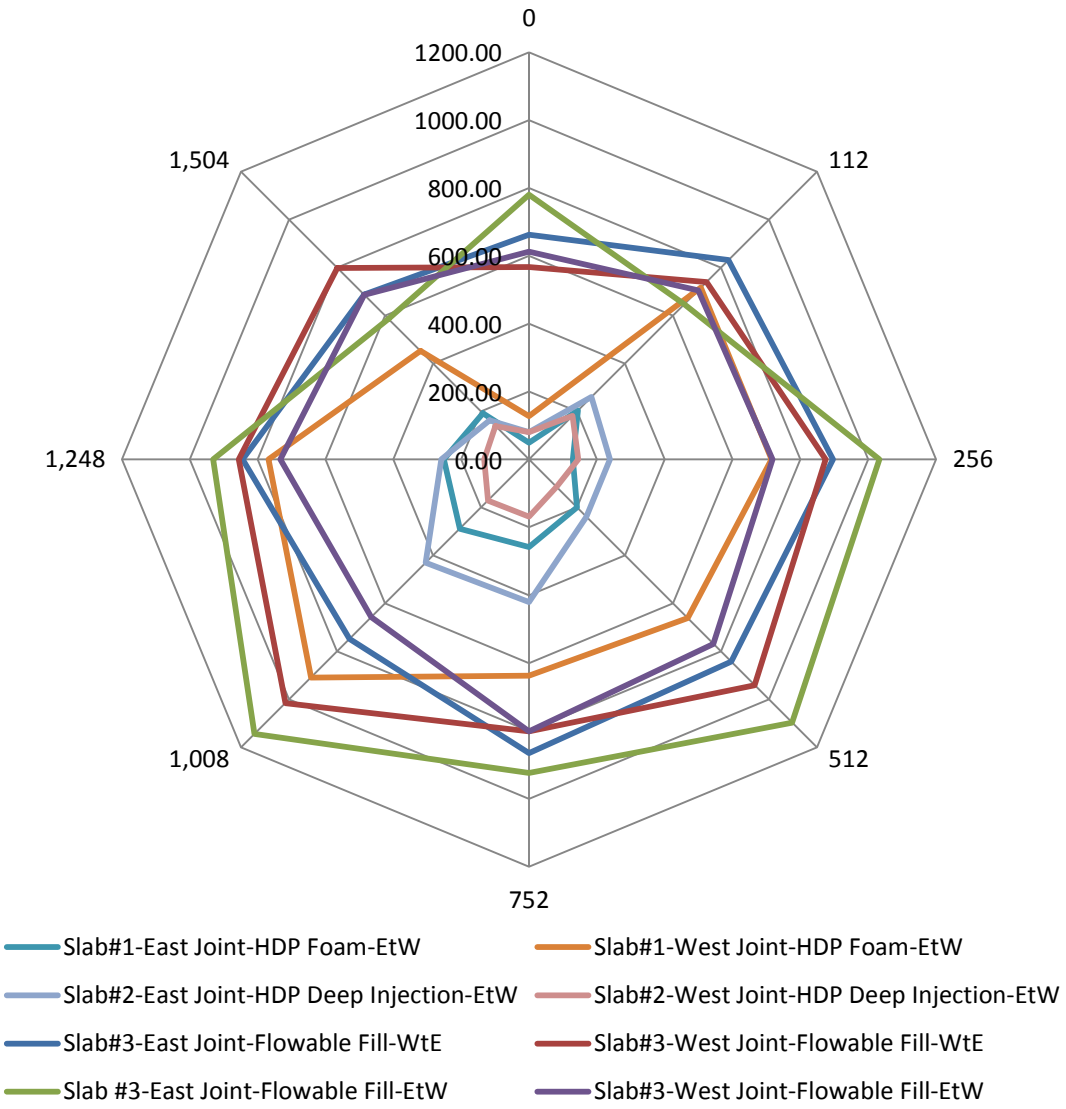

Figure – 46 Deformation Energy Analysis for Un-aged Concrete Slabs (8 Cases)

The deformation energy analysis for un-aged concrete slabs after several load applications of an F – 15 load cart resulted that the performance of slab #2, installed with deep injection and with west joints, was superior to the other eight cases. Slab #3 was founded to have the highest area in compared to the other variants; therefore, was ranked last in terms of deformation energy performance. Finally Slab # 1 performance in between slab #2 and #3.

5.2.4.2 Deformation analysis considering the Temperature Gradient

The three installation techniques were evaluated for concrete panels that had been exposed to environmental effects for a period of 2 years without any additional load applications on them. The purpose was to evaluate only the environmental effects and temperature distresses for the three installation techniques. Aging, curling and wrapping stresses, temperatures changes and other environmental parameters affecting the mechanical performance of the repair slabs for a period of two

years are reflected in this analysis. Four deformation energy analyses were performed for each concrete slab. The variation in the four analyses was the location of the joint (load transfer devices) and the direction of the traffic load. Figures 47, 48, 49, and 50 display the radar charts for each one of the four cases. Figures 47 and 48 represents two cases were the deformation energy was calculated with joints installed in the east side of the concrete slab; however, the load traveling direction varied. Case 1 in Figures 47 the performance was analyzed with the load traveling from east to west. Case 2 in Figure 48 the performance was analyzed with the load traveling from west to east. The two reminding cases out of the four are illustrated in Figures 49 and 50. In this two cases the joints were placed in the west side of the concrete repair slabs and the traveling direction of the load was alternated either going east to west or west to east. The effects in the deformation energy cause by the variation in the joint location and the traveling direction of the load are reflected in the radar charts below for each case.

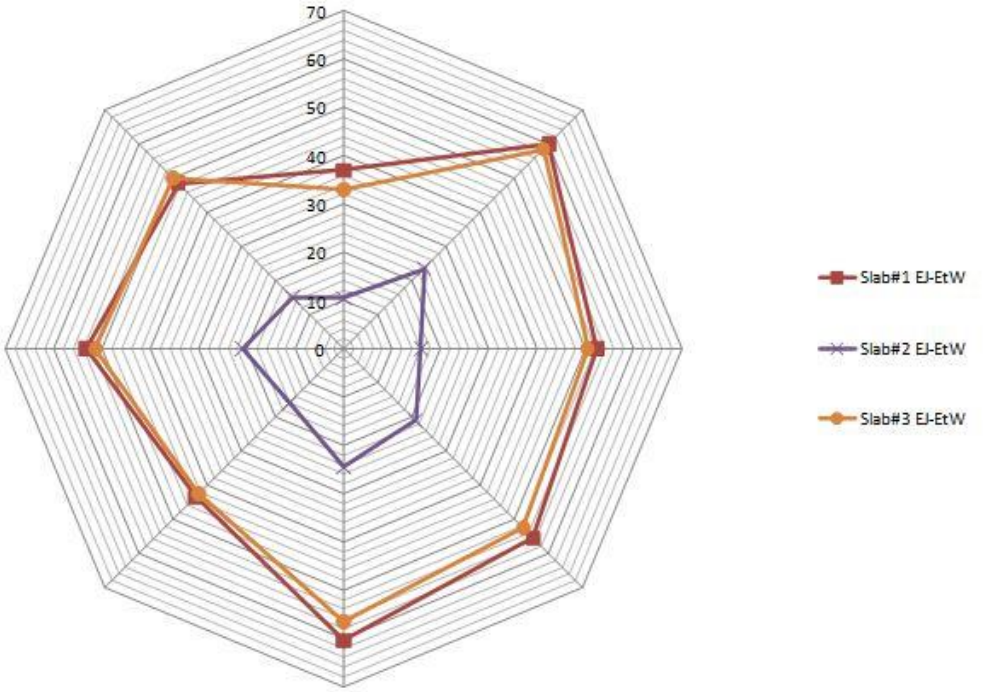

Figure – 47 Deformation Energy at the East Joint, Direction of Traffic East to West for the Three Slabs (Case 1)

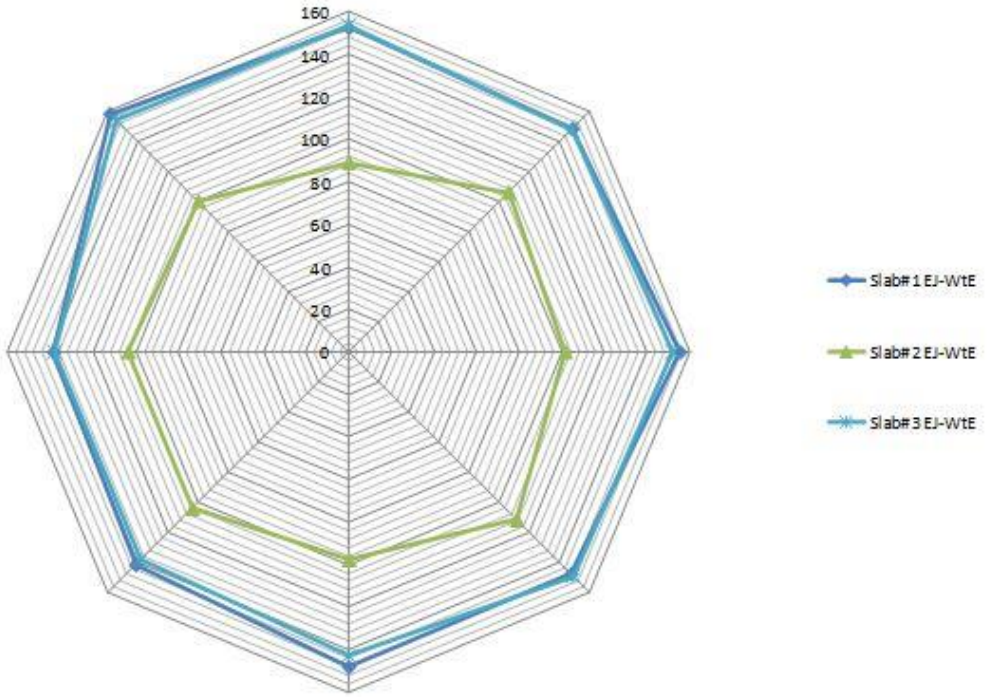

Figure – 48 Deformation Energy at the East Joint, Direction of Traffic West to East for the Three Slabs (Case 2)

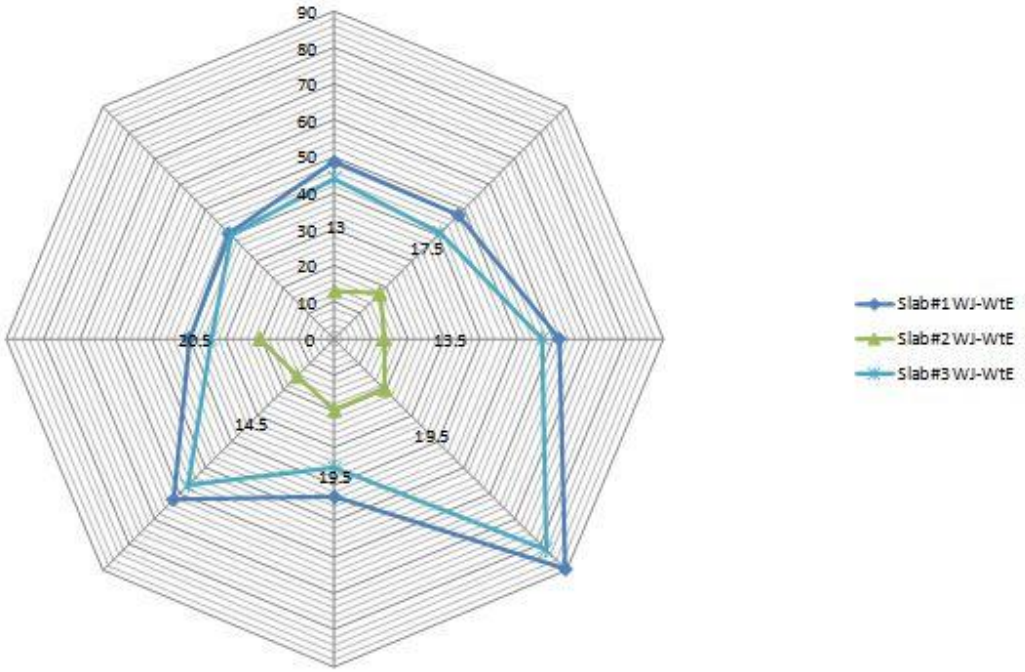

Figure – 49 Deformation Energy at the West Joint, Direction of Traffic West to East for the Three Slabs (Case 3)

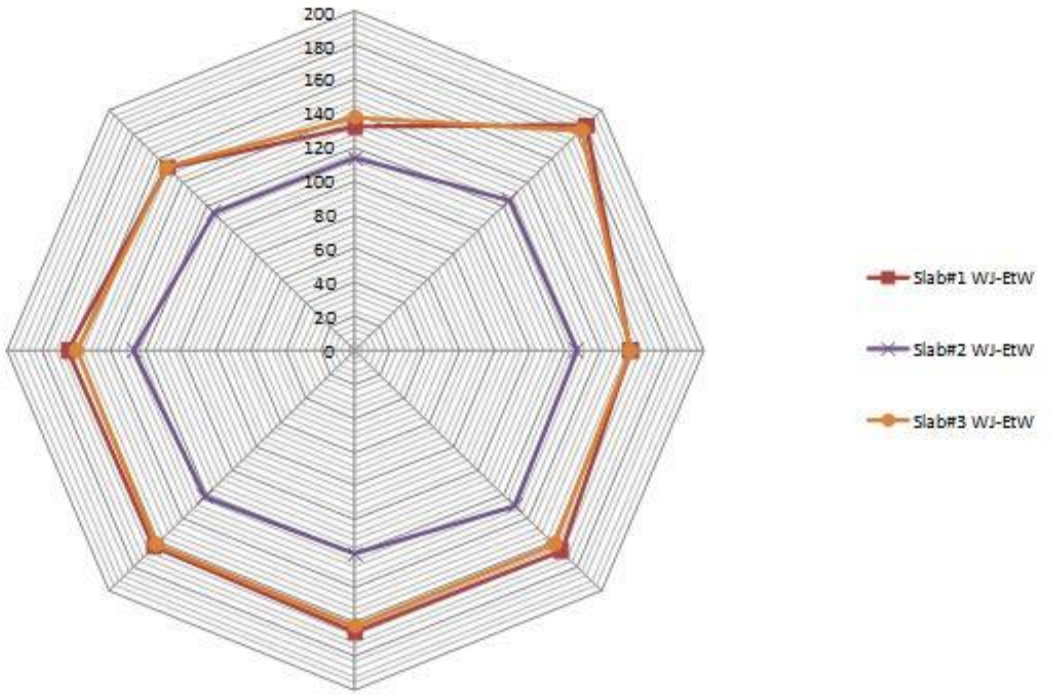

Figure – 50 Deformation Energy at the West Joint, Direction of Traffic East to West for the Three Slabs (Case 4)

In the Four cases shown in Figures 47, 48, 49 and 50, slab #2 had the smallest polygon areas in the radar charts. A smaller polygon area in the radar charts corresponds to systems with smaller values of deformation energy. Smaller differential deformation energy in turn, corresponds to systems that behave similarly at the two sides of the joints. As can be seem in the aforementioned plots, slab #2 had the best performance among the three slabs in terms of lower differential deformation energy. Slabs #1 and #3 proved to behave inferior compared to slab #2, installed using the deep injection of the high density polyurethane foam.

The location of the joint (load transfer devices) and the traveling direction of the load had a significant impact in the deformation energy. The deformation energy values were lower when the traveling direction of the load departure from the existing slab and approached the concrete repair slab compared to the cases when the traveling direction of the load departed the concrete repair slab and approach the existing slab. This relation can be illustrated by comparing the areas of each slab for the four cases. In other words, the value for the deformation energy was lower for the case of west joint location with load traveling from west to east or when the joints were located in the east side of the concrete repair panel and the load traveled from east to west. The deformation energy was worst when the joints were located in the west side of the concrete repair slab and the load traveled from east to west or when the joints were placed in the east side of the repair slab and the load traveled west to east. The joint location and load traveling are better illustrated in Figures 47 to 50.

5.3 Cost Analysis

The costs analysis for the repair of rigid pavements, consisted of expenditures associated with demolition, transportation of debris off-site, fabrication and construction of precast concrete panels, equipment rental, material purchases and hourly wages of the practitioners were considered to calculate the total cost of each precast concrete slab. The analysis was performed using the RS Mean 2013 cost data [16]. Additionally, the report "Evaluation of the URETEK Method of Pavement Lifting" [17] prepared by Wisconsin Department of Transportation was used to obtain the cost for the URETEK HDP foam. The cost analysis results are summarized and display in table 13.

Table 13. Summaries for the Cost Analysis Results

	Slab 1	Slab 2	Slab 3
Existing Slab Removal	$1,508	$1,508	$1,508
Precast Slab Construction	$490	$490	$532
Base Preparation and Installation	$1,862	$1,862	$1,572
Overall Cost	$3,860	$3,860	$3,611

The demolition process including saw cutting and removal of the damaged slabs was performed on relative bases for the three scenarios in the experiment design; therefore, the cost associated to the demolition and transportation of the shattered concrete off site are the same. A concrete saw was used to trim the existing slab. Initially the cost was obtained for cutting 3-inches in depth and every additional inch sawed after the third inch was added separately. Using the cost rates provided by RS means a total Cost of 264 dollars was calculated for each 10 by 10 ft. portion. Subsequently, a $1,245 cost for a 12-ton hydraulic crane was added as a 1-day rental expense. The rental cost included the labor and the equipment. The total cost associated with the saw cutting, demolition, and transportation of the excess materials was calculated as $1508. The precast concrete panels, namely slab 1 and slab 2, were constructed using a concrete mix that resulted the back-calculated modulus value of 5,000 psi, while the back-calculated modulus for the slab 3 turned out as 6,000 psi. The cost of the precast slab 1 and slab 2 resulted to be $490, and the fabrication and construction cost for precast slab 3 was calculated as $532. The costs include the concrete mixture, placing of concrete, reinforcement steel, and the dowels bars pre-fabricated in the precast concrete panels as load transfer mechanisms. Labor, material, and equipment required were considered in the costs.

The cost for the base preparation and installation of precast slab 1 and slab 2 come out to be $1,862. This cost include the rental expenses associated with obtaining a shovel/backhoe and hydraulic crane for 1-day. Additionally, the total calculated cost considers the expenditures on rental expense for a vibratory plate compactor, purchase of aggregates for the construction of the base layer, and costs pertaining to the application of URETEK HDP foam. The equipment required for the injection process of URETEK HDP foam consists of a pneumatic drill, an electric drill, a truck-mounted pumping unit for injection purposes, and a laser-leveling unit. It is imperative to state that the URETEK HDP foam costs were obtained from the report "Evaluation of the URETEK Method of Pavement Lifting" performed by Wisconsin Department of Transportation [17]. The cost for slab 3 base preparation and installation was calculated as $1,572. The process for the determination of the total cost for slab 3 was similar to slab 1

and slab 2; with the distinction of using a flowable fill as a cementitious leveling agent for the installation of the precast concrete panel. The overall cost, considering all components of the expenditures, for slab 1 and slab 2 was calculated to be $3,860, and the total cost for slab 3 was calculated as $3,611. The expenditures associated with the purchase of the materials, transportation, hourly wages of the practitioners, and equipment rental fees required to perform the work were considered to calculate the total cost. Appendix B provides specifics for the cost analysis of the precast concrete slabs.

6. Conclusion

This effort was aimed to provide a comparative study of the field performance of the precast concrete panels installed with different techniques. The slabs were installed using conventional injection of high density polyurethane (HDP) foam, deep injection of HDP foam, and flowable fill as leveling materials. The first portion of the report explains the influence of accelerated loading on the performance of repaired sections, immediately after construction. The performances of the slabs were characterized through their joint-load transfer efficiencies, joint stiffness, differential deformation energies, and the maximum plastic strains developed in the slabs using finite element simulations. The results of the un-aged precast panels clearly demonstrated that the concrete panels installed with deep injection of HDP foam performed superior in terms of lower differential deformation energy, better orthogonal load transfer efficiencies.

The second portion of the report discusses the influence of the climatic cycles, specifically temperature gradient and relative humidity, on the performance of the repaired sections. By the use of Heavy Weight Deflectometer (HWD), joint load transfer efficiencies after nearly two years were calculated during a hot summer day on a test pad in Florida. The temperature at the surface, mid-slab, bottom of the slab and four inches down in the subgrade layer were measured and used for the characterization of temperature dependency of the precast concrete panels installed using different leveling techniques. The mid-slab HWD drops were used to back-calculate the stiffness properties of the layers, namely modulus values, and the joint drops were used for the analysis of the load transfer efficiencies, as well as the differential deformation energy for each permutation of the experiment design. In addition to the direct field measurements, another performance criteria was employed to predict the field performance of the repaired sections. The strength ratio parameter, which is essentially the ratio of strength over maximum working stresses, was employed as a measure to characterize the likelihood of performance degradation in the repair sections. This measure basically identifies the proximity to the failure conditions; therefore systems with lower strength ratio are expected to be more prone to exhibit performance degradation during service life of the rigid pavements.

The results clearly showed the influence of a 35-degree temperature difference between the top and bottom fibers of the precast concrete panels. The finite element simulations were later used to determine the maximum vertical stresses and plastic deformations imposed at the top of the subgrade layer, as an additional measure of load distribution capacity of the repaired sections. The results of this analysis also seem to be in conformity with results of the load transfer efficiencies and the differential deformation energy analyses. Similar to the first segment of the report, the repair section installed using the deep injection of the HDP foam showed a superior performance compared to the other

counterparts. This could be attributed to the stabilization of the subgrade layer during the process of deep injection by providing a more robust platform for the installation of the repair section.

7. Recommendations

A layer elastic analysis was performed in this study. Calculations were made assuming a layer elastic model for the unbounded granular base layer and for the subgrade. The environmental and load accumulation analysis were performed with this assumption. Layered elastic modeling of pavement foundation results in unrealistic tensile stresses at the bottom of the subgrade and base layer. Investigation in modeling pavement system have discover that anisotropic modeling of granular material develops a more realistic stress and strain under the load [15]. The granular layer should be characterized as an anisotropic model for more realistic results.

The installation of the precast concrete panels required the removal of the distressed portion of slab. A walk-behind saw and a wall-saw were used to trim the damaged portion of slab. In the time comparison the walk-behind outperformed the wall by a significant amount of time; therefore, a walk-behind with help of skilled personal is recommend to be used when removing the slab to reduce the time of slab removing.

8. References

[1] Voigt, G.F., “Fast Full-Depth Pavement Repair,” Report RP334P, American Concrete Pavement Association.

[2] Olidis, Chris, Swan, D.J., Saeed, Athar, et al., “Repair of Airfield Rigid Pavements Using Concrete Panels,” Technical Report AFRL.RX.TY.2009-4588, Tyndall Air Force Base, Air Force Research Lab Materials and Manufacturing Directorate, 2009.

[3] Ashtiani, R., Jackson, C., Saeed, A., & Hammons, M. (2010). Precast Concrete Panels for Contingency Rigid Airfield Pavement Damage Repair.

[4] An Overview of the Super-Slab® System. Fort Miller Co. [Online] [Cited February 2, 2010.] www.super-slab.com

[5] Hossain, S., Ozyildirim, C., and Tate, T.R., “Evaluation of Precast Patches on U.S. 60 Near the New Kent and James City County Line,” Report VTRC 06-R22, Virginia Transportation Research Council, 2006.

[6] Pavement Lifting. UretekUSA Co. [Online] [Cited February 16,2010] www.uretekusa.com

[7] Swift Lift® System. Dayton Superior. [Online] [Cited March 5, 2010] www.daytonsuperior.com

[8] Hammons, M.I. and A. M. Ioannides,” Advanced Pavement Design: Finite Element Modeling for Rigid Pavement Joints. Report I: Background Investigation”, DOT/FAA/AR-97-7, 1998.

[9] Khazanovich L. and Gotlif A. “Evaluation of Joint and Crack Load Transfer – Final Report”, FHWA-RD-02-088, 2003.

[10] ARA, Inc. “Guide for Mechanistic- Empirical Design of New and Rehabilitated Pavement Structures,” NCHRP 1-37A Report, Appendix JJ “Transverse Joint Faulting Model” Transportation Research Board, National Research Council, Washington, D.C. 2004

[11] Crovetti J.A. & Darter M.I. ; “Void Detection for Jointed Concrete Pavements” Transportation Research Record 1041, Transportation Research Board, National Research Council, Washington, D.C. 1985, pp. 3-11.

[12] VanWick, A., Larralde, J., Lovell, CW and Chen, WF, “Development of a Pumping Prediction Model”, ASCE Journal of Transportation Engineering, 115, 2, March, 1989 pp. 161–175.

[13] Larralde, J. and Chen, WF, “Estimation of Mechanical Deterioration of Highway Rigid Pavements”,

ASCE Journal of Transportation Engineering, 113, 2, 1987, pp. 193–207

[14] Bhatti, M.A., Barlow, J.A., and Stoner, J.W. “Modeling Damage to Rigid Pavements Caused by Subgrade Pumping,” ASCE, Journal of Transportation Engineering, Vol. 122, No. 1, Jan-Feb 1996, pp. 12-21.

[15] Ashtiani, R., D. N. Little, E. Masad, “Material Factors That Influence Anisotropic Behavior of Aggregate Bases”, Transportation Research Record No. 2059, Transportation Research Board, 2008, Washington, D.C., pp 20-30.

[16] *RSMeans building construction cost data 2013 (71st annual ed.). (2012). Norwell, MA: RSMeans.*

[17] Abu al-Eis, K., & LaBarca, I. (2007). Evaluation of The URETEK Method® of Pavement Lifting. 30-30. Retrieved from http://wisdotresearch.wi.gov/wp-content/uploads/wi-02-07uretekmethod1.pdf

9. Appendices

Appendix A
Load Transfer Efficiency

Table AA-1 Slab #1 Load Transfer Efficiency,
East Joint, Load Traveling East to West

Pass #	D_1	D_2	LTE_δ	LTE_σ	LTE*
0	16.56	15.57	0.94	0.97	0.5
112	21.25	17.16	0.81	0.89	0.35
256	19.61	17.02	0.87	0.93	0.41
512	21.15	17.16	0.81	0.9	0.35
752	22.67	17.51	0.77	0.87	0.31
1008	22.72	16.95	0.75	0.85	0.3
1248	21.49	16.48	0.77	0.87	0.35
1504	20.83	16.99	0.82	0.9	0.36

Table AA-2 Slab #1 Load Transfer Efficiency,
West Joint, Load Traveling East to West

Pass #	D_1	D_2	LTE_δ	LTE_σ	LTE*
0	18.13	15.58	0.86	0.92	0.4
112	34.43	20.1	0.58	0.74	0.19
256	29.27	14.97	0.51	0.68	0.16
512	28.76	15.54	0.54	0.7	0.17
752	39.83	27.08	0.68	0.81	0.25
1008	37.89	19.72	0.52	0.68	0.16
1248	31.65	16.29	0.51	0.68	0.16
1504	24.89	15.84	0.64	0.78	0.22

Table AA-3 Slab #2 Load Transfer Efficiency,
East Joint, Load Traveling East to West

Pass #	D_1	D_2	LTE_δ	LTE_σ	LTE*
0	17.83	16.22	0.91	0.95	0.45
112	22.8	17.59	0.77	0.87	0.31
256	20.99	16.21	0.77	0.87	0.31
512	21.15	16.37	0.77	0.87	0.31
752	29.44	21.03	0.71	0.83	0.27
1008	25.97	17.36	0.67	0.8	0.24
1248	21.6	16.43	0.76	0.86	0.3
1504	20.39	17.12	0.84	0.91	0.38

Table AA-4 Slab #2 Load Transfer Efficiency,
West Joint, Load Traveling East to West

Pass #	D_1	D_2	LTE_δ	LTE_σ	LTE*
0	17.36	15.74	0.91	0.95	0.45
112	22.44	18.8	0.84	0.91	0.38
256	19.7	16.8	0.85	0.92	0.39
512	19.63	17.34	0.88	0.94	0.42
752	26.55	23.18	0.87	0.93	0.41
1008	22.99	19.57	0.85	0.92	0.39
1248	20.5	17.85	0.87	0.93	0.41
1504	20.11	17.32	0.86	0.93	0.4

Table AA-5 Slab #3 Load Transfer Efficiency,
East Joint, Load Traveling West to East

Pass #	D_1	D_2	LTE_δ	LTE_σ	LTE*
0	33.31	20.06	0.6	0.75	0.2
112	34.76	18.13	0.52	0.69	0.16
256	38.35	20.43	0.53	0.7	0.17
512	36.55	19.7	0.54	0.7	0.17
752	35.35	18.04	0.51	0.68	0.16
1008	35.94	20.98	0.58	0.74	0.19
1248	35.38	18.5	0.52	0.69	0.16
1504	33.91	20.17	0.59	0.75	0.2

Table AA-6 Slab #3 Load Transfer Efficiency,
West Joint, Load Traveling West to East

Pass #	D_1	D_2	LTE_δ	LTE_σ	LTE*
0	32.26	20.91	0.65	0.79	0.23
112	30.96	16.16	0.52	0.69	0.16
256	35.21	17.72	0.5	0.67	0.15
512	35.75	16.94	0.47	0.64	0.14
752	29.84	13.82	0.46	0.63	0.14
1008	37.52	17.21	0.46	0.63	0.14
1248	30.88	13.78	0.45	0.62	0.13
1504	30.04	14.07	0.47	0.64	0.14

Table AA-7 Slab #3 Load Transfer Efficiency,
East Joint, Load Traveling East to West

Pass #	D_1	D_2	LTE_δ	LTE_σ	LTE*
0	36.01	20.4	0.57	0.72	0.19
112	28.97	16.02	0.55	0.71	0.18
256	38.31	17.65	0.46	0.63	0.14
512	39.07	17.13	0.44	0.61	0.13
752	32.68	14.2	0.43	0.61	0.13
1008	41.47	18.59	0.45	0.62	0.13
1248	32.93	14.32	0.43	0.61	0.13
1504	29.15	17.43	0.6	0.75	0.2

Table AA-8 Slab #3 Load Transfer Efficiency,
West Joint, Load Traveling East to West

Pass #	D_1	D_2	LTE_δ	LTE_σ	LTE*
0	36.64	24.39	0.67	0.8	0.24
112	30.29	16.19	0.53	0.7	0.17
256	37.06	22.71	0.61	0.76	0.21
512	37.35	21.98	0.59	0.74	0.2
752	31.69	15.67	0.49	0.66	0.15
1008	37.61	24.47	0.65	0.79	0.23
1248	31.06	16.41	0.53	0.69	0.17
1504	30.11	16.38	0.54	0.7	0.17

Appendix B

Cost Analysis

RS Mean ID	Desciption	Number	Unit	Base Material	Base Labor	Base Equipment	Bare Total	Quantity	Total
3811350400	3" deep slab Concrete Saw	1	L.F.	0.17	0.81	0.65	1.63	40	$65
3811350420	Additional inch of Concrete Saw	9	L.F.	0.06	0.27	0.22	0.55	40	$198
15419500100	12-ton tuck-mounted hydraulic crane	1	days		390	855	1245	1	$1,245
Existing Concrete Slab Portion Removal Total Cost									$1,508
33105350400	5000 psi Concrete	1	CY	108			108	2.7778	$300
33105704300	Placing Concrete over 6" thick direct chute	1	CY		16.15	0.6	16.75	2.7778	$47
32110600600	Uncoated Reinforcing Steel #3 to #7	1	Tons		1000	695	1695	0.03384	$57
32110602430	Dowels #8	1	Each	1.65	2.21		3.86	20	$77
32110602450	Add for Dowels	1	Lb	0.55	1.1		1.65	5.34	$9
Precast Concrete Slab 1 and 2 Construction Total Cost									$490
33105350411	6000 psi Concrete	1	CY	123			123	2.7778	$342
33105704300	Placing Concrete over 6" thick direct chute	1	CY		16.15	0.6	16.75	2.7778	$47
32110600600	Uncoated Reinforcing Steel #3 to #7	1	Tons		1000	695	1695	0.03384	$57
32110602430	Dowels #8	1	Each	1.65	2.21		3.86	20	$77
32110602450	Add for Dowels	1	Lb	0.55	1.1		1.65	5.34	$9
Precast Concrete Slab 3 Construction Total Cost									$532
15433203860	Rent shovel/backhoe bucket 0.5 CY	1	days			66.5	66.5	1	$67
15419500100	12-ton tuck-mounted hydraulic crane	1	days		390	855	1245	1	$1,245
30513251050	Aggregate Stone 3/4" to 1-1/2"	1	CY	38.5			38.5	1.86	$72
30513251100	Add for Transportation 10-mile round trip	1	CY		6.1	14.45	20.55	1.86	$38
15433201350	Rent Vibratory Plate Compactor 5000lb blow	1	days			32.5	32.5	1	$33
WDT Report	URETEK HDP Foam	1	Lb				7	58.333	$408
Base Preparation and Installation for Slab 1 and 2									$1,862
15433203860	Rent shovel/backhoe bucket 0.5 CY	1	days			66.5	66.5	1	$67
15419500100	12-ton tuck-mounted hydraulic crane	1	days		390	855	1245	1	$1,245
30513251050	Aggregate Stone 3/4" to 1-1/2"	1	CY	38.5			38.5	0.926	$36
30513251100	Add for Transportation 10-mile round trip	1	CY		6.1	14.45	20.55	0.926	$19
15433201350	Rent Vibratory Plate Compactor 5000lb blow	1	days			32.5	32.5	1	$33
33105350300	4000 psi Concrete Flowable Fill	1	CY	102			102	1.39	$142
33105704600	Placing Concrete 4 1/2" thick direct chute	1	CY		10.8	0.4	11.2	2.7778	$31
Base Preparation and Installation for Slab 3									$1,572